Remodeling Jellyfish

Thesis by
Mengsha Gong

In Partial Fulfillment of the Requirements for the
Degree of
Doctor of Philosophy

Caltech

CALIFORNIA INSTITUTE OF TECHNOLOGY
Pasadena, California

2022
Defended November 1st, 2021

ACKNOWLEDGEMENTS

Many thanks to the following people, without whom this thesis would probably not exist.

Lea Goentoro, for her insatiable curiosity about the little wonders in biology, and for her insistence on precision and rigor. Without that insistence, my intuition for how things work would not have been put into so many words, and this thesis would have been weaker for it.

My committee members, Michael Elowitz, Rob Phillips, and Michael Dickinson for their invaluable perspective whenever I was in too deep and for their unwavering belief that this work was interesting and worth pursuing.

The Jelly Team of the Goentoro Lab, especially Mike Abrams, Misha Raiffee, and Ty Basinger, for teaching me about jellyfish and grafting, for keeping the jellies alive, and for general goofs and entertainment.

The Caltech ballroom community, for reminding me of the greater world out there of which science is only a part, for feelings of progression and satisfaction when research gave me none, for keeping me in shape, and for being a place for me to use my brain in a different way.

My parents, for understanding what it takes to get a PhD, for their patience and endless support, and for never asking why I hadn't graduated yet.

My husband Sean, of course, for keeping me sane between thesis writing sessions, for commiserating, for keeping me fed, and for utter dependability.

And lastly to Cairo, who gave me the deadline I needed and just about guaranteed that this thesis would be completed, even if it was like pulling teeth. Mom loves you so much already.

ABSTRACT

Why are jellyfish round? Circularity facilitates many physiological functions in jellyfish like the moon jelly *Aurelia aurita*, including swimming and feeding. Previous work suggests that *Aurelia* might maintain its circularity through its muscle contractions. We use grafting experiments to investigate how these muscle contractions regulate shape in *Aurelia* and find that the same mechanism *Aurelia* uses to quickly recover circularity after it is injured can also produce square, oval, and triangular jellyfish. We then turn to modeling to ask what characteristics of the jellyfish muscle contractions and body materials give *Aurelia* the capability to reorganize its shape. Our simulations suggest that *Aurelia* body shape is a dynamic equilibrium that is not only reorganized by periodic muscle contractions when it is disrupted, but is also reinforced by the same muscle contractions over the course of normal physiological function.

TABLE OF CONTENTS

LIST OF ILLUSTRATIONS

C h a p t e r   1

INTRODUCTION

1.1   Significance

Animals are built *de novo* during development. Cell proliferation, differentiation, patterning, and morphogenesis come together in concert and generate a vast diversity of animal forms and shapes from single cells. In many animals, body shape is further remodeled post-development during metamorphosis or regeneration. During these periods, body structures are removed either by internal or external factors, such as apoptosis or injury, and as during development, cell proliferation, differentiation, patterning, and morphogenesis activate to generate new body shapes and structures (Ishizuya–Oka, Hasebe, and Shi, 2010; Tattamanti et al., 2019; Gurtner et al., 2008). Body shape tends to be fixed in adult animals that have completed development and metamorphosis, and the standard alternative to regeneration is that the structure and function are not recovered and that the injured shape is maintained rather than repaired. How adult animal shape is regulated during the course of normal physiological function, or if animal shape is actively regulated at all, has not been explicitly studied.

Our current understanding of how shapes and structures are formed in animals suggests that animal shape is likely dynamically regulated rather than static. Modern models of morphogenesis posit that shape formation is regulated through self-organization in conjunction with the more traditional paradigm of positional information. The self-organizing mechanisms that have been identified as drivers of both pattern formation and shape generation during morphogenesis and development can take many forms. Interactions like local cell signaling, differential adhesion, co-ordinated apical constriction, and differential growth-driven mechanical buckling work in tandem with positional information to guide cell behavior during developmental processes as varied as cell fate determination (Werner, Vu, and Rink, 2016), cell sorting (Winklbauer and Parent, 2017; Amack and Manning, 2012; Lecuit and Lenne, 2007), invagination (Lecuit and Lenne, 2007), tissue branching (Varner et al., 2015), and the formation of villi (Shyer et al., 2013), cortical convolutions (Tallinen et al., 2016; Garcia, Kroenke, and Bayly, 2018; Llinares–Benadero and Borrell, 2019), and gut loops (Savin et al., 2011; Schweisguth and Corson, 2019; Green

and Sharpe, 2015). Experiments have shown that cells and tissues have inherent self-organizing properties, even when isolated from their native environments that might provide external signalling or global feedback (Lefevre et al., 2017; Galliot, 2012; Werner, Vu, and Rink, 2016).

Self-organization—the formation and regulation of global structures, patterns, and behaviors through simple local interactions—is a defining feature of complex systems like those found at every hierarchical level in biological systems. During self-organization, simple rules govern the behavior of individual components and, through feedback loops and iteration, allow complex and diverse phenomena to emerge from disorder. Turing famously illustrates this in his 1952 paper, *The Chemical Basis of Morphogenesis*, where he described how a simple interaction between two molecules where one inhibits the other as they spatially diffuse can form oscillations and standing waves by magnifying minute variability between cells (Turing, 1952). This simple set of interactions—a reaction diffusion system—has been shown to be able to produce patterns as varied as zebra stripes, cheetah spots, and more intricate patterns like those found on seashells (Murray, 1988; Meinhardt, 1995). Sets of simple rules like this govern the organization of microtubules into a spindle during mitosis and the formation of individual fish and birds into fluid yet cohesive murmurations and shoals (Brugues and Needleman, 2014; Katz et al., 2011; Attanasi et al., 2015).

One key characteristic of self-organization is that the interactions that form the global pattern or structure do not cease after the pattern or structure is formed. Instead, the interactions are ongoing, resulting in a continuously regulated dynamic, yet stable, pattern or structure. This dynamicism facilitates self-repair as perturbances are driven back toward the stable state and also allows biological systems to respond flexibly to stimulus and changing environmental conditions, since small tweaks to the rules that govern local interactions can result in dramatic global changes. We see this in examples of self-organization on many other scales in biology. On a microscopic scale, continuous assembly and disassembly of microtubules results in asters, vortices, and spindles depending on the tubulin monomer to motor protein ratio and the presence of chromosomes (Nédélec et al., 1997; Surrey et al., 2001; Brugues and Needleman, 2014). On a macro scale, a school of fish becomes more cohesive in the presence of a predator as each individual seeks to be closer to its neighbors (Tien, Levin, and Rubenstein, 2004; Katz et al., 2011).

Drawing parallels from these self-organized systems, we expect the patterns and structures generated though self-organization during development and morphogenesis to also be dynamic and continuously regulated. While there are no obvious examples of continuous dynamic regulation in self-organized shapes and structures as of yet, there do exist examples of this in self-organized patterns. Studies have shown evidence that the striped patterns of zebrafish are still regulated by self-organization post-development. In zebrafish, the stripes are hypothesized to be self-organized via diffusion reaction, and Yamaguchi et al. have shown that when these stripes are disrupted by laser irradiation, the pattern is dynamically repaired (Yamaguchi, Yoshimoto, and Kondo, 2007). Continuous regulation of animal shape post-development has not been explicitly studied however. Investigation of shape repair in animals has focused on processes like regeneration, which are driven by the initiation of additional developmental processes, rather than ongoing mechanisms that may also reinforce and maintain shape in the absence of injury. Discovery of a new mechanism of shape repair in *Aurelia* that does not rely on regenerative processes gave us an opportunity to explore how shape might be regulated throughout the lifetime of an animal.

1.2 *Aurelia aurita* **and symmetrization**
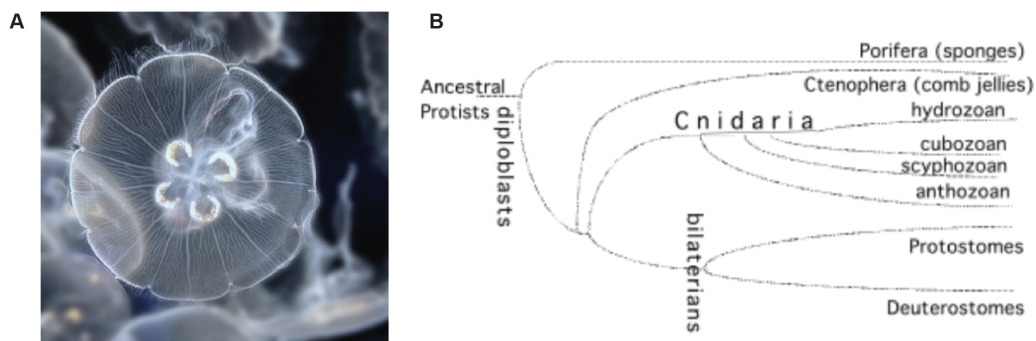
Figure 1.1: *Aurelia aurita*. A. *Aurelia aurita*, like all members of the phylum Cnidaria, are characterized by radial symmetry. Image © Jill Odice Photography. B. Cnidaria are a sister phylum to bilaterians, and consist of four classes. *Aurelia aurita* are members of Scyphozoa. Taken from (Galliot and Schmid, 2002)

Aurelia aurita, the moon jelly, are a member of Cnidaria, a sister phylum to Bilaterians that includes jellies, corals, anemone, and hydra (Figure 1.1). Cnidarians are characterized by radial symmetry, soft bodies bolstered by a layer of extracellular matrix called mesoglea, and stinging cells called cnidocytes (R. Brusca and G. Brusca, 2003). Cnidarians are known for their regenerative abilities, and many

cnidarians, most notably the freshwater polyp Hydra, have been models for regeneration ever since 1744 (Trembley, 1744). It is with some surprise, therefore, that some cnidarians, including *Aurelia aurita*, do not regenerate lost body parts upon injury, but rather recovers using a novel mechanism (Abrams et al., 2015).

In 2015, Abrams et al. discovered that, rather than regrowing lost body parts upon amputation, *Aurelia aurita* redistribute the body parts that remain and recover radial symmetry (Abrams et al., 2015). In *Aurelia*, radial symmetry is crucial for facilitating swimming and feeding behaviors. This process, named symmetrization, robustly allows animals to recover radial symmetry within 48 hours. Abrams et al. hypothesize that radial symmetry facilitates growth and maturation of ephyra into medusa, as the animals that fail to symmetrize also fail to develop normally.

Abrams et al. found that symmetrization does not depend on cellular processes such as cell proliferation and apoptosis. Instead, symmetrization is driven by muscle contraction and viscoelastic response from the mesoglea. Muscle contractions compress the mesoglea. When the muscles relax, the elastic recoil of the mesoglea causes the body tissue to pivot into the cut site, redistributing the tissues until radial symmetry is restored. Symmetrization was originally described in juvenile *Aurelia* (ephyra). We have found that adult *Aurelia* (medusa) have the same capability for symmetrization (Figure 1.2).
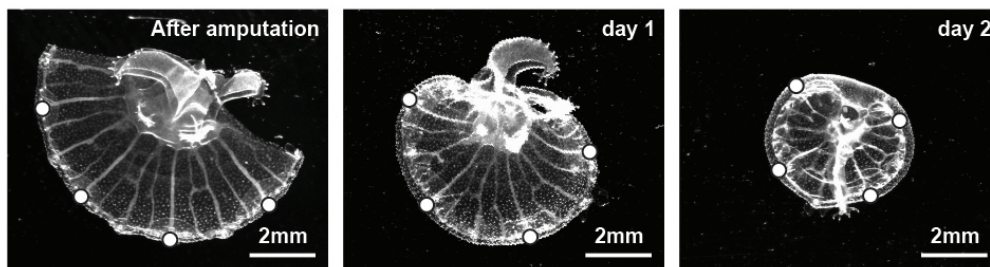
Figure 1.2: *Aurelia* medusa symmetrize and recover radial symmetry upon amputation. Medusa that were cut in half recover radial symmetry over the course of 2 days. Body tissues (tracked by white dots) pivot about the manubrium until tissues are redistributed evenly.

1.3 Thesis overview

Discovery of a novel mechanically-driven strategy for recovering radial symmetry raises many questions. How does the animal sense when radial symmetry is broken and when it is recovered? Is symmetrization regulated through global feedback or

local interactions? In this thesis, I take advantage of this novel mechanism to ask whether body shape is dynamic throughout the lifetime of this animal, and how it is regulated if that is the case.

In Chapter 2, we use an experimental approach to probe the extent of shape reorganization in *Aurelia aurita*. Using grafting, we rearranged the muscle and bulk tissue into different configurations to explore the extent of shape self-repair and found, surprisingly, that the normal swimming contractions that drive recovery of radial symmetry can also reorganize *Aurelia* into other stable body shapes, such as oval, triangular, and square depending on the initial geometric and muscle configuration. We find that the underlying muscle also reconnects and reorganizes, resulting in the emergence of novel swimming behaviors. Our results support the hypothesis that swimming actively regulates *Aurelia* body shape, and that radial symmetry may be a dynamic equilibrium in a system with many possible solutions. The presence of these novel jellyfish shapes suggests that muscle-driven shape regulation in *Aurelia* is more flexible than previously thought, and might be a more general mechanism for shape reorganization rather than a mechanism specific to recover of radial symmetry.

There is a limit to the questions we can answer through grafting experiments, however, due to lack of tools for manipulation of mechanical parameters *in vivo*. So in Chapter 3, we turn to modeling to explore how these mechanical forces might be interacting to drive shape reorganization. We designed a coarse-grained finite-element model describing the local mechanical interactions between muscle contraction and viscoelastic response. We describe an incremental approach that can be used to model systems where the forces acting on the system depend on the state of the system and that accomodates large deformations. By excluding any forces that might be present due to cellular processes or global feedback, we assessed the extent to which local interactions drive shape reorganization in *Aurelia*. Modeling also allowed us to explore the effects of mechanical parameters such as muscle force, stiffness, and viscosity on *Aurelia* shape change.

We discuss the results of our model simulations in Chapter 4. We found that a certain amount of fluidity in the body tissue is required to recapitulate reorganization. We also found that local interactions are not only sufficient to recapitulate *Aurelia* shape reorganization, but that the same parameter sets can explain reorganization into different stable solutions, including oval, rectangular, and S-shapes, depending on the initial geometry of the simulated jellyfish. We argue that the stability of these shapes, despite the continued simulation of forces, supports our hypothesis

that jellyfish shape are dynamic equilibria of a self-organizing system. We find that mechanical parameters like muscle contraction rate and contraction strain not only affect the reorganization rate of *Aurelia*, but can also determine which shape solutions are accessible to the system.

Finally, in Chapter 5, we discuss future directions for this work and the potential for our findings in *Aurelia* to inspire the creation of synthetic shape-changing materials.

References

Abrams, Michael et al. (2015). "Self-repairing symmetry in jellyfish through mechanically driven reorganization." In: *PNAS* 112, E3365–E3373.

Amack, Jeffrey D. and M. Lisa Manning (2012). "Knowing the boundaries: extending the differential adhesion hypothesis in embryonic cell sorting." In: *Science* 338, pp. 212–215.

Attanasi, Alessandro et al. (2015). "Emergence of collective changes in travel direction of starling flocks from individual birds' fluctuations." In: *Journal of The Royal Society Interface* 12, p. 20150319.

Brugues, Jan and Daniel Needleman (2014). "Physical basis of spindle self-organization." In: *PNAS* 111, pp. 18496–18500.

Brusca, Richard and Gary Brusca (2003). *Invertebrates*. 2nd ed. Sinauer Associates.

Galliot, Brigitte (2012). "Hydra, a fruitful model system for 270 years." In: *The International Journal of Developmental Biology* 56, pp. 411–423.

Galliot, Brigitte and Volker Schmid (2002). "Cnidarians as a model system for understanding evolution and regeneration." In: *The International Journal of Developmental Biology* 46, pp. 39–48.

Garcia, Kara E., Christopher D. Kroenke, and Philip V. Bayly (2018). "Mechanics of cortical folding: Stress, growth and stability." In: *Philosophical Transactions of the Royal Society B* 373, p. 20170321.

Green, Jeremy B.A. and James Sharpe (2015). "Positional information and reaction-diffusion: two big ideas in developmental biology combine." In: *Development* 142, pp. 1203–1211.

Gurtner, Geoffrey et al. (2008). "Wound repair and regeneration." In: *Nature* 453, pp. 314–321.

Ishizuya–Oka, Atsuko, Takashi Hasebe, and Yun–Bo Shi (2010). "Apoptosis in amphibian organs during metamorphosis." In: *Apoptosis* 15, pp. 350–364.

Katz, Yael et al. (2011). "Inferring the structure and dynamics of interactions in schooling fish." In: *PNAS* 108, pp. 18720–18725.

Lecuit, Thomas and Pierre-François Lenne (2007). "Cell surface mechanics and the control of cell shape, tissue patterns and morphogenesis." In: *Nature* 8, pp. 633–644.

Lefevre, James G. et al. (2017). "Self-organisation after embryonic kidney dissociation is driven via selective adhesion of ureteric epithelial cells." In: *Development* 144, pp. 1087–1096.

Llinares–Benadero, Cristina and Víctor Borrell (2019). "Deconstructing cortical folding: Genetic, cellular and mechanical determinants." In: *Nature Neuroscience* 20, pp. 161–176.

Meinhardt, Hans (1995). *The algorithmic beauty of sea shells.* Springer, Berlin, Heidelberg.

Murray, James D. (1988). "How the leopard gets its spots." In: *Scientific American* 258, pp. 80–87.

Nédélec, François J. et al. (1997). "Self-organization of microtubules and motors." In: *Nature* 389, pp. 305–308.

Savin, Thierry et al. (2011). "On the growth and form of the gut." In: *Nature* 476, pp. 57–62.

Schweisguth, François and Francis Corson (2019). "Self-organization in pattern formation." In: *Developmental Cell* 49, pp. 659–677.

Shyer, Amy et al. (2013). "Villification: How the gut gets its villi." In: *Science* 342, pp. 212–218.

Surrey, Thomas et al. (2001). "Physical properties determining self-organization of motors and microtubules." In: *Science* 292, pp. 1167–1171.

Tallinen, Tuomas et al. (2016). "On the growth and form of cortical convolutions." In: *Nature Physics* 12, pp. 588–593.

Tattamanti, Gianluca et al. (2019). "Autophagy in development and regeneration: role in tissue remodelling and cell survival." In: *The European Zoological Journal* 86, pp. 113–131.

Tien, Joseph H., Simon A. Levin, and Daniel I. Rubenstein (2004). "Dynamics of fish shoals: Identifying key decision rules." In: *Evolutionary Ecology Research* 6, pp. 555–565.

Trembley, Abraham (1744). *Mémoires pour servir à l'histoire d'un genre de polypes d'eau douce, à bras en forme de cornes.*

Turing, Alan (1952). "The chemical basis of morphogenesis." In: *Philosophical Transactions of the Royal Society B* 641, pp. 37–72.

Varner, Victor et al. (2015). "Mechanically patterning the embryonic airway epithelium." In: *PNAS* 112, pp. 9230–9235.

Werner, Steffen, Hanh Thi–Kim Vu, and Jochen C. Rink (2016). "Self-organizatino in development, regeneration and organoids." In: *Current Opinion in Cell Biology* 44, pp. 102–109.

Winklbauer, Rudolf and Serge E. Parent (2017). "Forces driving cell sorting in the amphibian embryo." In: *Mechanisms of Development* 144, pp. 81–91.

Yamaguchi, Motoomi, Eiichi Yoshimoto, and Shigeru Kondo (2007). "Pattern regulation in the stripe of zebrafish suggests an underlying dynamic and autonomous mechanism." In: *PNAS* 104, pp. 4790–4793.

Chapter 2

AURELIA REORGANIZE TO STABLE NOVEL BODY SHAPES WHEN MUSCLE AND BULK TISSUE ARE REARRANGED

2.1 Introduction

How animal shape is created during morphogenesis is a question that has long fascinated biologists, but how animal shape is regulated over the lifetime of an animal is not a question that is explicitly asked. Animals might repair or regenerate appendages or structures over the course of their lifetimes when these structures are injured or lost, but we do not typically consider this shape regulation. This might be because the benefit of expending so much energy to repair or regenerate structures lies in the recovery of function, and we do not associate animal shape as important for function.

In *Aurelia aurita*, however, body shape plays an important role in many physiological functions. Radial symmetry is thought to facilitate omni-directional sensing and interaction with the environment (R. Brusca and G. Brusca, 2003). Furthermore, the circular bell and muscle ring in *Aurelia* medusa are crucial to swimming, feeding, and reproduction. Body shape regulation and repair should therefore convey many benefits to *Aurelia aurita*, and indeed, Abrams et al. discovered that *Aurelia* quickly and robustly recover radial symmetry after injury, after which the animals are able to swim, feed, and mature normally (Abrams et al., 2015). Intriguingly, this recovery process, termed symmetrization, is driven mechanically through muscle contractions rather than through regenerative processes. These muscle contractions are used for propulsion in the absence of injury, which made us wonder if body shape might be continuously regulated in *Aurelia* as a part of normal physiological function. By exploring the dynamics of the mechanics driving symmetrization, we hope to shed some light on how animal shape is regulated throughout the lifetime of an animal.

The moon jelly, *Aurelia aurita*, is a member of Cnidaria, a phylum that includes corals, sea anemone, and many jellyfish (Figure 2.1). Cnidarian life cycles can have up to two adult forms—the sessile polyp and the free-swimming medusa. *Aurelia aurita* has both. The polyps reproduce asexually via budding, and under certain circumstances (seasonally in the wild, and when induced chemically or via temperature shock in the lab), via strobilation, during which a single polyp produces
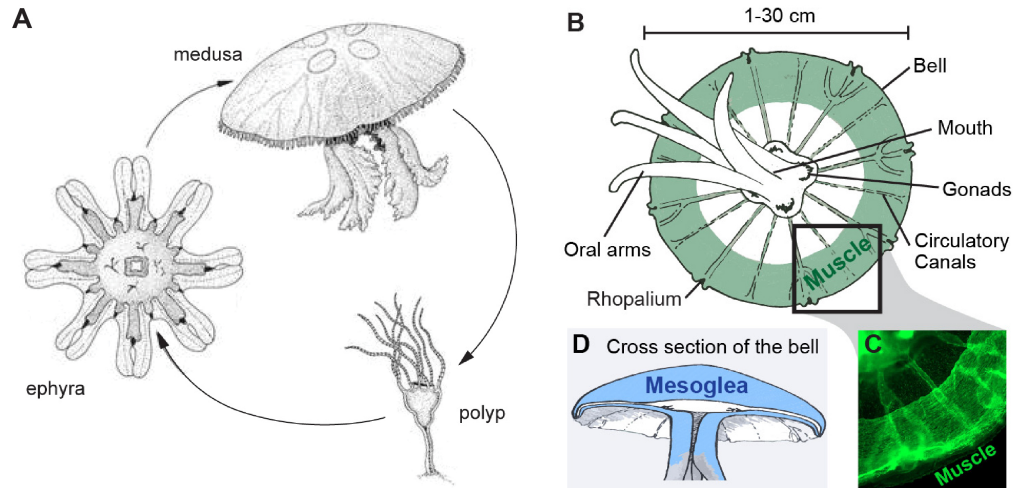
Figure 2.1: *Aurelia* life cycle and anatomy. A. A simplified diagram of the *Aurelia* life cycle. The sessile adult stage (polyp) undergoes strobilation to produce the benthic juvenile stage (ephyra), which then matures into the benthic adult stage (medusa). Medusa reproduce sexually to produce planular larvae (not shown) which settle and develop into polyps (adapted from (R. Brusca and G. Brusca, 2003)). B. Diagram of *Aurelia* medusa as seen from the subumbrella. *Aurelia* have a radially symmetrical bauplan with a circular muscle band lining the subumbrellar side of the bell (green shading). Eight sensory organs (rhopalia) are distributed around the rim of the bell. Extending from the center of the bell are four oral arms which converge at a mouth surrounded by four crescent-shaped gonads inside the gastric pouches. Circulatory canals extend radially from the mouth to the periphery of the bell. C. The muscle band of a young *Aurelia* medusa stained with phalloidin. D. Diagram of a cross-section of the *Aurelia* medusa bell. The epidermis lines the ex- and subumbrella of the bell. The gastrodermis lines the interior of the gastric pouches and circulatory canals. In between these tissue layers is the mesoglea (shaded in blue).

many juvenile jellyfish called ephyra (R. Brusca and G. Brusca, 2003; Fuchs et al., 2014). These ephyra mature into adults called medusa. Medusa reproduce sexually and the fertilized eggs develop into planula, small larvae that settle into the ocean floor and develop into the polyp stage, starting the cycle again (Figure 2.1A). In this work, we study the body shape regulation in medusa.

Aurelia medusa have a saucer-shaped bell. Members of Cnidaria have a radially symmetric body plan consisting of two tissue layers (epidermis and gastrodermis) that sandwich between them a layer of viscoelastic extracellular matrix called mesoglea (R. Brusca and G. Brusca, 2003). In *Aurelia*, the gastrovascular cavity takes the form of four gastric pouches in a clover configuration that surround a mouth and

oral arms located at the center of the underside (subumbrella) of the bell. A flat ring of muscle lines the periphery of the bell subumbrella. Rather than having a centralized nervous system, *Aurelia* have sensory centers called rhopalia are spaced periodically along the edge of the bell (Figure 2.1 B-C). The motor nerve net transmits pacemaker signals from the rhopalia to the muscle ring (Gladfelter, 1972; Arai, 1997). To swim, the muscle ring contracts like a drawstring, expelling water from the bell and compressing the layer of viscoelastic mesoglea. When the muscles relax, the mesoglea elastically rebounds, returning the bell and muscle to their initial expanded shape (Gemmell et al., 2013). During symmetrization, the same muscle contractions that propel *Aurelia* during swimming drive recovery of radial symmetry by pushing viscoelastic tissues into the injured or cut site where there is least resistance (Abrams et al., 2015).

In a system where shape recovery is mechanically driven, might body shape also be mechanically encoded? Abrams et al. found that *Aurelia* can recover radial symmetry from amputations as extreme as quartering, which suggests that very little tissue is required to encode and fully recover animal shape. Are specific tissues or tissue interactions required to encode animal shape? By exploring how *Aurelia* shape responds to various interactions between the mechanical elements that drive shape recovery—the force-producing muscle and viscoelastic tissue—we hope to shed light on how these mechanical elements regulate body shape. Amputation has an inherent limitation in that tissue can only be removed, which restricts the extent to which new interactions can be tested. Luckily, *Aurelia* are amenable to grafting, which allows us to test more extensive perturbations and rearrangements of the muscle and tissue.

2.2 Recovery of radial symmetry is robust to reconfiguration of muscle and body geometry

What happens to *Aurelia* shape when the mechanical machinery that drives symmetrization is rearranged? How might *Aurelia* respond to more extreme deviations from radial symmetry? We considered three possibilities. First, perhaps *Aurelia* are able to recover radial symmetry from any body geometry. We can imagine that a system primarily driven by global minimization, such as one in which muscle contraction increases the pressure inside the jellyfish body which then acts to evenly redistribute the tissue, might produce circularity as the only stable shape. Second, perhaps *Aurelia* are only able to recover radial symmetry when its mechanical elements are rearranged into certain configurations and does not change shape when

the requirements for shape recovery are not met. This might be the case if specific interactions between mechanical elements are required to drive any kind of shape change, for example if symmetrization only occurs when the muscle band pushes the tissue around the mouth. In this regime, we would expect no shape change to occur if the mouth were removed or if the orientation of the muscle band were disrupted. A third possibility is that *Aurelia* might also be able to reorganize its body into non-circular shapes depending on the arrangement of its mechanical machinery. For example, if jellyfish tissue is locally rearranged by muscle contraction into the nearest region of least resistance, we might expect non-circular jellyfish shapes to be stable as long as forces are locally balanced. To test these hypotheses, we turned to grafting.

Figure 2.2 illustrates how medusa pieces were grafted together. To produce precise geometric pieces, we drew templates on graph paper, placed them underneath the anesthetized medusa, and cut along the templates. Medusa pieces were then arranged in the desired configuration and pinned with cactus spines on an agarose bed (Bickell–Page and Mackie, 1991). Within 24 hours, the pieces fused together, were unpinned, and taken out of anesthetics, upon which the chimeras resumed pulsation (Movie S1). Fusion occurred regardless of whether pieces from the same animal or from different animals were grafted together. We were thus able to explore how *Aurelia* respond to a wide range of rearrangements and configurations using tissue from two or more animals.
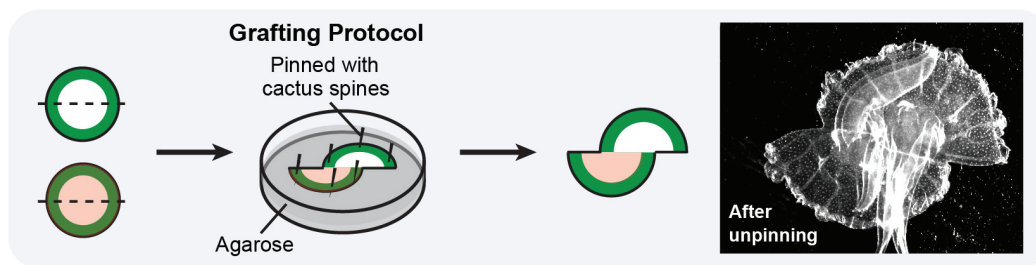
Figure 2.2: Grafting protocol. Left: Anesthetized *Aurelia* medusa are cut in the desired shapes and arranged into the desired graft configurations on an agarose bed, where they are pinned in place with cactus spines overnight (muscle ring represented in green). After the pieces fuse together, the pins are removed. The chimera is then removed from anesthetic. Muscles resume contractions less than 24 hours post-surgery. Right: An offset graft immediately after unpinning.

Aurelia recovered radial symmetry from a wide range of graft geometries. Chimeras stabilized into a circular shape from semicircular pieces grafted with an offset (Figure 2.3A, n=22), semicircles grafted orthogonally, three alternating quarters, three pieces in a row, and even three pieces in a pinwheel (Figure 2.3B). Shape reorganization occurred within 1-4 days. Immediately after grafting, muscle bands on different pieces contracted independently. However, during the course of reorganization, neighboring muscle bands gradually began to contract synchronously. The frequency of synchronous contraction increased until the muscle bands behaved as a single muscle ring and pulsed indistinguishably from uncut medusa. The mouths on separate medusa pieces also tended to converge toward the center of the chimera.

These experiments showed that *Aurelia* display a remarkable ability to not only recover radial symmetry from injuries that could feasibly occur in nature, but also to recover its shape even from highly unnatural perturbations that dramatically rearrange the relative configuration of the muscle and bell tissues. The robust ability to recover radial symmetry might have evolved to allow for rapid recovery of the characteristic drawstring-like contraction of the circular muscle band that generates fluid flow of water into the the bell subumbrella, pulling food toward the oral arms and propelling *Aurelia* medusa forward (Dabiri et al., 2005).
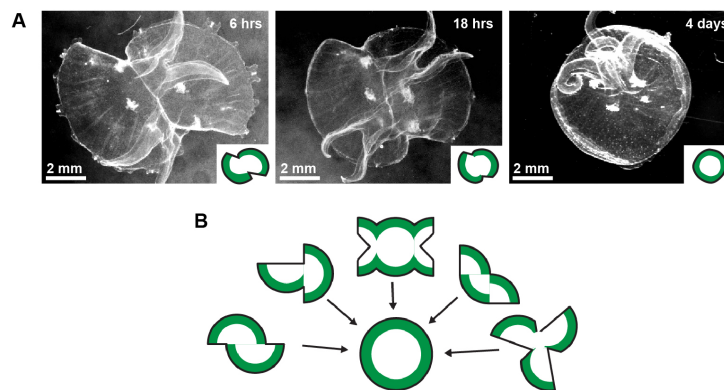
Figure 2.3: *Aurelia* chimerae are able to recover radial symmetry from a wide range of graft configurations. A. Two medusa pieces grafted in an offset are imaged 6 hours, 18 hours, and 4 days after unpinning. Cartoons at the bottom right corner show the shape of the graft at each time point with estimated muscle band position shaded in green. B. Five graft configurations that successfully recovered radial symmetry, with muscle bands shaded in green.

2.3 *Aurelia* can reorganize their bodies into stable shapes that are not radially symmetrical

However, the grafting experiments also provided a surprising result. Many graft configurations resulted in chimera that reorganized into altogether different stable shapes, such as ovals, triangles, and squares (Figure 2.4A-C). Some of these graft configurations involved only small changes to the ones that produced round shapes. In the offset graft, increasing the offset distance of the two semicircles resulted in oval jellyfish (Figure 2.4D). In the butterfly graft, decreasing the relative size of the middle piece also resulted in oval jellyfish, decreasing it further resulted in rectangular and trapezoidal jellyfish, and removing the middle piece altogether resulted in square jellyfish (Figure 2.4E-F). Pinwheel grafts in which the length of the pinwheel spokes was decreased reorganized into triangular jellyfish (Figure 2.4G). In offset grafts with very high offset distances, we observed that chimerae no longer reorganized into ovals. These animals, along with chimerae composed of two quarter pieces grafted together in an offset, reorganized into S-shaped animals with rotational symmetry. These grafts exhibited reorganization analogous to what we observed in the pinwheel grafts, and could be considered two-spoke pinwheels.

Results from the offset graft were especially striking, as there was no clear delineation between grafts that recovered radial symmetry and those that reorganized into oval animals. Instead, increasing the offset distance of the two semicircular pieces resulted in animals that ranged continuously from circular to elongated ovals (Figure 2.4H). Achieving these novel shapes, in particular the oval and trapezoid, required substantial changes from the initial graft geometry, which suggested active reorganization toward these novel shapes rather than simply a failure to recover radial symmetry.

Reorganization in offset grafts took between 1-4 days to achieve an oval or circular shape, while pinwheel and butterfly grafts took longer, reorganizing to trapezoid, square, and triangular shapes within 10 days (Supplementary Figure 2.12). However, there was the possibility that after an initial dramatic reorganization phase, the jellyfish chimera might continue to change shape more gradually. An oval jellyfish, for example, may become circular given enough time. To assess whether these novel body shapes were stable, we tracked individual rectangular (n=5) and oval (n=13) jellyfish and found that body shape was stable for over a month (Supplementary Figure 2.13), which is of the same order of magnitude as the lifespan of *Aurelia* in

the wild. This suggests that the novel body shapes are not just intermediate states for chimera that have yet to recover circularity, but rather are stable states.

Finally, we observed a lack of preference for circularity. Rather, the initial graft geometry is predictive of the final shape of the animal (Figure 2.4I). For instance, two semicircular pieces grafted back to back reorganized consistently into square animals, and we observed a clear correlation between the initial offset distance of the offset graft and the final aspect ratio of oval jellyfish post-reorganization. Multiple initial graft geometries can converge to the same final shape, for instance, oval animals emerged from offset grafts and many variations on the butterfly graft. In conjunction with evidence that the final shape is dependent on the initial graft geometry, this suggests that jellyfish body shape is a dynamical system with multiple stable solutions. The final shapes observed also suggested that stable solutions may all fall into a few categories with radial, bilateral, and rotational symmetries.
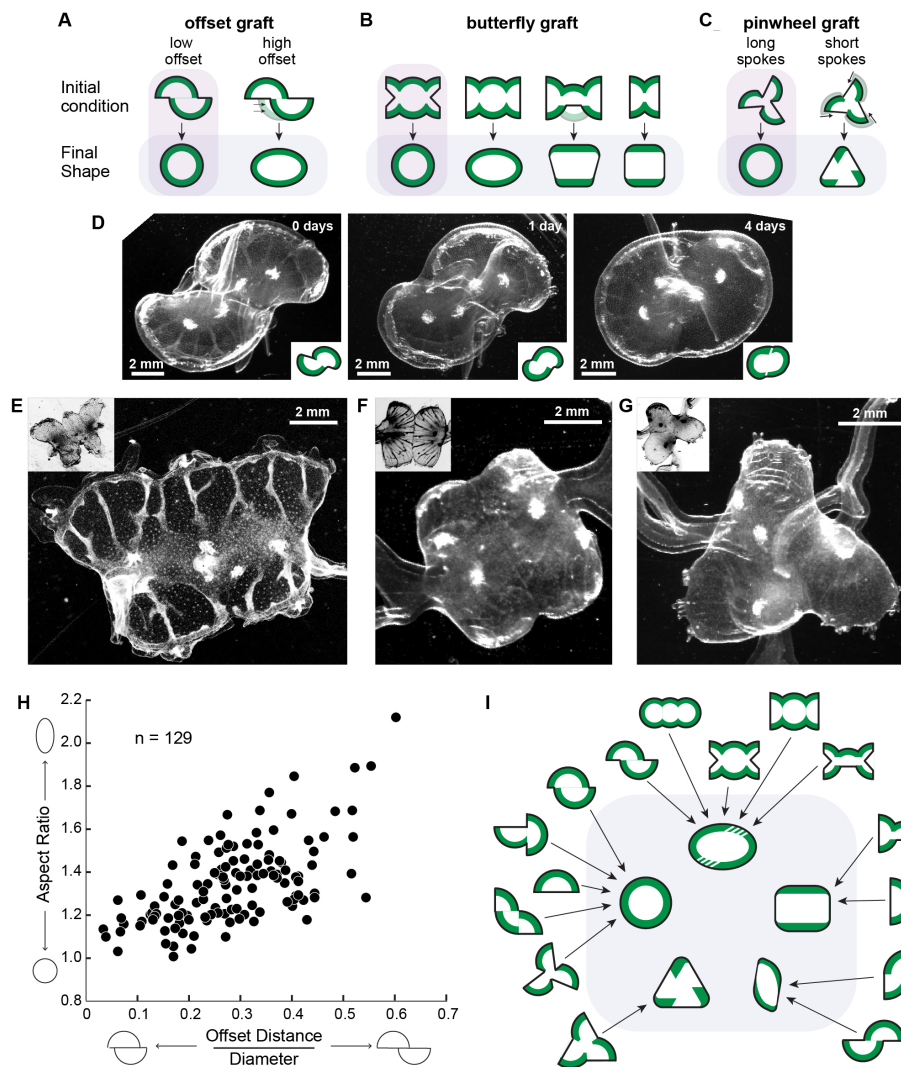
Figure 2.4: *Aurelia* chimera reorganize to different body shapes depending on initial graft geometry. A. Offset grafts with increased offset distance reorganized into oval jellyfish. B. Butterfly grafts where the size of the side piece is increased reorganized into oval jellyfish. Decreasing the size of the center piece resulted in trapezoidal or rectangular jellyfish, and removing the center piece altogether resulted in square jellyfish. C. Pinwheel grafts where the length of each spoke is decreased reorganized into triangular jellyfish. D. An offset graft imaged immediately, 1 day, and 4 days post-surgery. The cartoon next to each image represents the shape of the graft at each time point, with muscles shaded in green. E. A fully reorganized trapezoidal, F. square, and G. triangular jellyfish with their respective initial graft configurations in the top left corner. H. The aspect ratio of the stable circular and oval jellyfish shapes post-reorganization of offset graft correlates with the initial offset distance. The offset distance was measured on day 0 post-surgery. The aspect ratio was

Figure 2.4: measured on day 3-4 post-surgery. The data comes from 24 experiments. I. Multiple initial graft geometries can converge to the same outcomes (grey box). Green shading indicates muscle patterns as indicated by phalloidin staining or deduced from observations of muscle contractions. The shapes included here are by no means exhaustive.

2.4 Non-circular chimerae adjust behaviors and tissue organization to body shape

As with the chimerae that recovered radial symmetry, neighboring muscle pieces in non-circular chimerae also synchronized over the course of several days. Some oval jellyfish recovered a drawstring-like swimming contraction (Movie S2, and Figure 2.5). Interestingly, we also observed clamshell and flapping swimming behaviors in oval and rectangular animals, respectively, that successfully propelled the animals forwards, though not as effectively as the wild-type behavior in uncut medusa (Movie S3-S4, Figure 2.6, Figure 2.7). Although mouth pieces in oval and rectangular animals did not converge as in circular chimera, we still observed prey capture and food in the gastric pouches of these animals over the course of a month of tracking. The animals also grew or maintained their size during this time, in sharp contrast to animals which were starved and shrank over time. In contrast to observations in amputation experiments that animals that do not recover radial symmetry fail to mature properly, chimera that did not recover radial symmetry did still recover function to some extent and maintained body proportions comparable to healthy uncut medusae.

Not all chimera exhibited muscle synchronization however. Muscle pieces that were not physically adjacent, like those in triangular and S-shaped jellyfish as well as some in rectangular jellyfish, did not synchronize and muscle pieces contracted independently of each other throughout the course of reorganization. (Movie S5). While muscle contractions still occurred in these animals, they did not exhibit effective swimming behavior, suggesting that muscle lengths below a certain threshold cannot effectively be used for propulsion and that the formation of muscle connections and synchronized contraction might be necessary for recovery of swimming function.

The alternative swimming behaviors suggest that muscles and nerves reorganized to accommodate the new body shapes. To verify this, we used actin and antibody stains to visualize the muscle band and motor nerve net in reorganized chimerae. We found that over the days-long process of reorganization, neighboring muscle
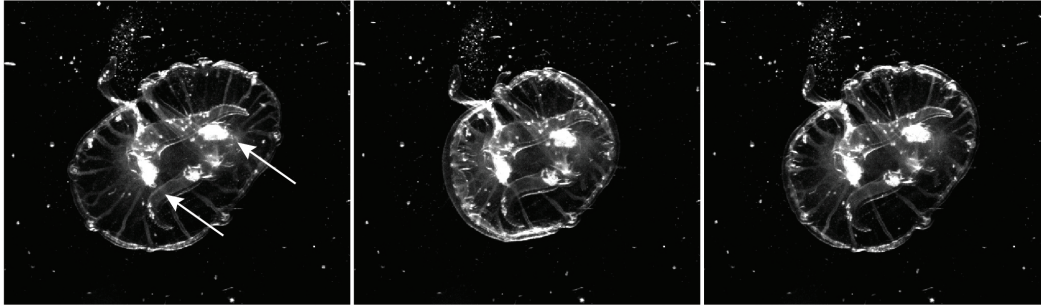
Figure 2.5: Offset graft that reorganized into an oval jellyfish with synchronized drawstring-like contractions. Timelapse images show one full contraction cycle. Food (brine shrimp, white arrows) can be seen in the two gastric pouches.
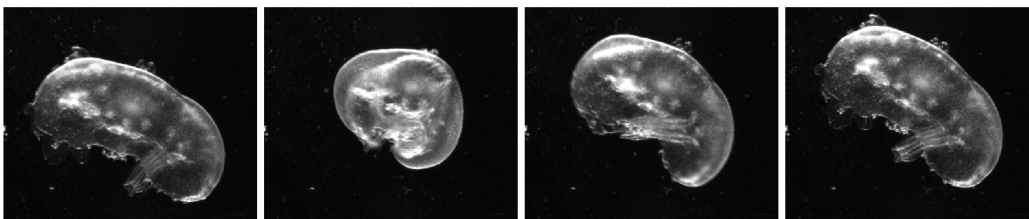
Figure 2.6: Three pieces grafted linearly that reorganized into an oval jellyfish with clamshell-like swimming behavior. Timelapse images show one full contraction cycle in which the animal propels itself slightly across the field of view.
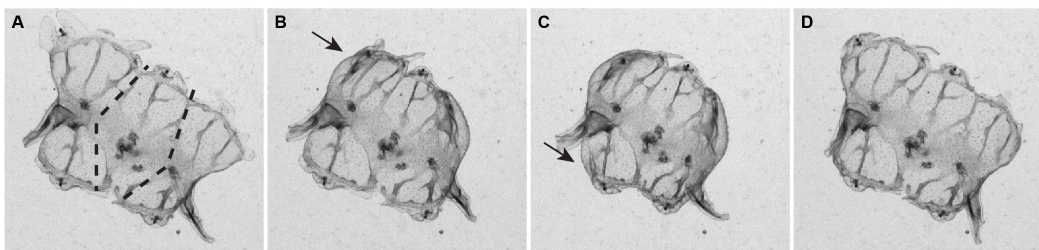
Figure 2.7: A butterfly graft that reorganized into a trapezoidal jellyfish with flapping swimming behavior with two synchronized muscle bands. Time-lapse images show one full contraction cycle. A. Fully relaxed trapezoidal jellyfish. Dashed lines approximate the original cut sites of the graft. B. The top muscle band (arrow) initiates contraction while the bottom muscle band is still relaxed. C. The bottom muscle band (arrow) initiates contraction while the top muscle band begins to relax. D. Both muscle bands in the process of relaxing.

bands and nerve nets fully reconnected across the cut site such that no break can be seen (Figure 2.8A). The muscles reorganized to accommodate the new body shapes according to the patterns of synchronous contraction we observed in the grafted animals. Circular and oval chimerae had continuous muscle rings about the bell
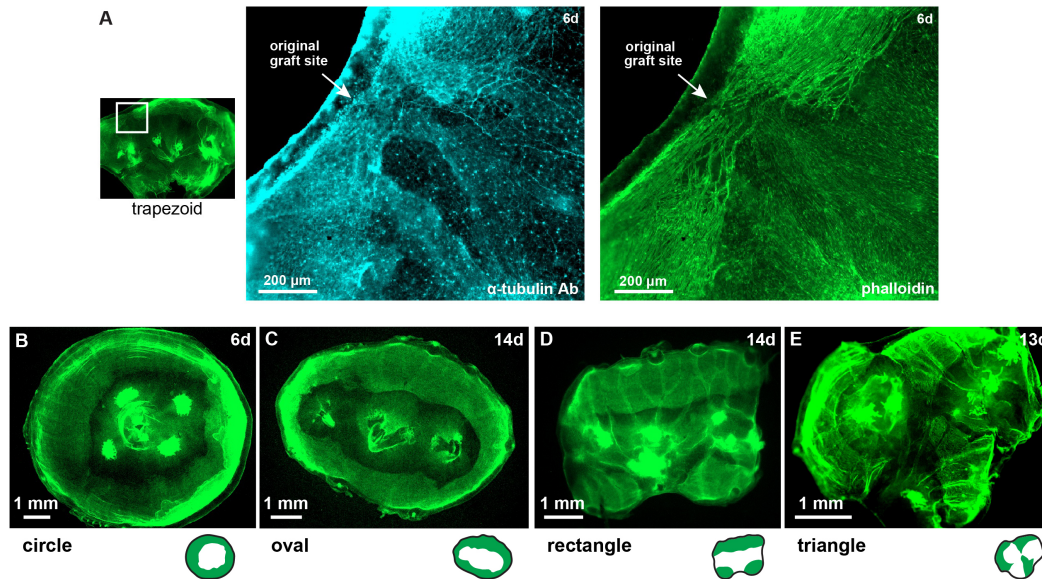
Figure 2.8: Molecular staining shows reformed muscle and nerve connection between grafted pieces and reorganization of muscle to accommodate new body shapes. A. A zoom-in of a graft site from a trapezoid chimera at 6 days post-surgery. The motor nerve net, stained using anti-tyrosinated-α-tubulin antibody (blue), is connected across the original graft site. Actin staining using phalloidin (green) shows blunt cut edges of muscle with actin fibers beginning to reconnect across the original graft site. B. Phalloidin staining of an offset graft 6 days post-surgery showing a reconnected circular muscle ring. C. Phalloidin staining of a butterfly graft 14 days post-surgery showing a reconnected oval muscle ring. D. Phalloidin staining of a butterfly graft 14 days post-surgery showing three linear muscle bands. E. Phalloidin staining of a pinwheel graft 13 days post-surgery showing three muscle bands radiating out from the center.

periphery (Figure 2.8B-C). Trapezoid and rectangular animals had a linear muscle band along the top edge and either a second parallel muscle band along the bottom edge or a distinct muscle piece in each bottom corner depending on whether the muscle pieces along the bottom row connected successfully (Figure 2.8D). Pinwheel grafts had muscle bands that radiated outward in spokes. These muscles were short and straight in triangular chimerae and curved in circular chimerae (Figure 2.8E). The ability of the muscle pieces to readily form connections to neighboring pieces and reorganize their configuration, and therefore swimming behavior, are a testament to the flexibility of *Aurelia* shape reorganization.

The emergence of novel muscle configurations with novel swimming behaviors made us wonder if body shapes with symmetry—radial, bilateral, or rotational—might

provide better swimming function, and if there might be some mechanism of global feedback that drives reorganization toward symmetrical body shapes. We found, however, that alongside symmetrical body shapes, *Aurelia* chimera readily reorganized into asymmetrical shapes. We observed part-round, part-polygonal animals that reorganized from offset, butterfly, and pinwheel grafts (Figure 2.9A-C). Each spoke of a pinwheel graft, for example, seems to decide independently of the others whether to reorganize into a rounded or polygonal shape. The underlying muscle of these animals, too, reorganized asymmetrically, forming configurations where some muscle pieces reconnected but not others (Figure 2.9D). We hypothesize that these asymmetrical animals are a result of local asymmetries present in the initial graft geometry. These local asymmetries might be the result of imprecise cuts that are unavoidable when performing surgery of small, slippery animals and, in the case of performing grafts with pieces from multiple animals, inherent size differences between animals. These asymmetrical animals provide evidence against the presence of strong global feedback, but rather support that both shape reorganization and muscle reconnection are regulated locally.
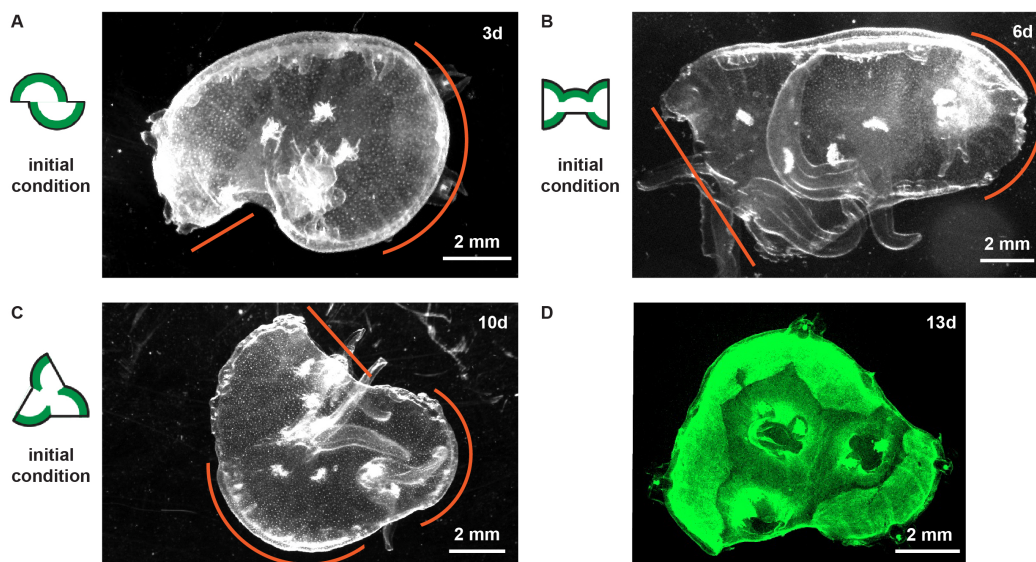
Figure 2.9: Grafts can result in asymmetrical jellyfish body shapes. A. Some offset grafts reorganized into half-oval, half-S-shaped animals (n=26). B. Some butterfly grafts reorganized into half-oval, half-trapezoids (n=5). C. Some pinwheel grafts reorganized into triangles with both rounded and sharp corners (n=6). D. Phalloidin stain of a pinwheel graft at 13 days after unpinning with both rounded and sharp corners showing two muscle pieces which have reconnected and one muscle piece which has not.

2.5 Shape reorganization is driven by muscle contraction and viscoelastic response

Is the mechanism of muscle contraction and viscoelastic response that drives recovery of radial symmetry during symmetrization also able to drive reorganization into non-circular body shapes? Alternatively, perhaps grafting invokes a different response than amputation, and non-circular body shapes are formed by a different process entirely.

To determine whether reorganization is dependent on muscle contraction, we tested whether reorganization still occurred when muscle contractions were inhibited with 0.8mM menthol in artificial seawater (ASW), which has been used as both an anesthetic and muscle relaxant in marine invertebrates (Gaudioso et al., 2012; Abrams et al., 2015; Norton et al., 1996). We observed no measurable muscle contractions in offset grafts that were kept in menthol solution, and these grafts showed no global shape reorganization over two days of tracking. (Figure 2.8A) To confirm these results, we tested inhibiting muscle contraction with another molecule, 2,3-Butanedione monoxime (BDM), which is a muscle-specific type II myosin inhibitor (Higuchi and Takemori, 1989). Offset grafts kept in 30mM BDM in artificial seawater also displayed no global reorganization over two days. The only change we observed in these muscle-inhibited offset grafts was some minimal local boundary smoothing (Supplementary Figure 2.14), suggesting the presence of some local tissue relaxation independent of muscle contraction.

These experiments suggest that reorganization to non-circular shapes requires muscle contraction. To test this finding, we tested the effects of increasing the muscle contraction rate of offset grafts by decreasing the magnesium concentration in the media. Magnesium ions decrease muscle excitability and magnesium concentration has been used to modulate muscle contraction previously in *Aurelia aurita* ephyra, where it was found that the animals recovered radial symmetry more quickly when muscle contraction was increased by reduction of magnesium concentration (Fawcett, Haxby, and Male, 1999; Abrams et al., 2015). Magnesium ion concentration was reduced in the media by 25% by mixing magnesium-free ASW with regular ASW in a 1:3 ratio. Contraction rates of offset grafts placed in this media increased from 25 to 28 contractions per minute on average and the animals reorganized more quickly than offset grafts in ASW, with 74% of animals in reduced-magnesium ASW completing reorganization by day 2 compared to 32% of animals in regular ASW (Figure 2.8B). That reorganization does not occur in the absence of muscle con-

traction and that reorganization rate correlates directly with muscle contraction rate implies that muscle contraction is the primary driver of *Aurelia* shape reorganization.
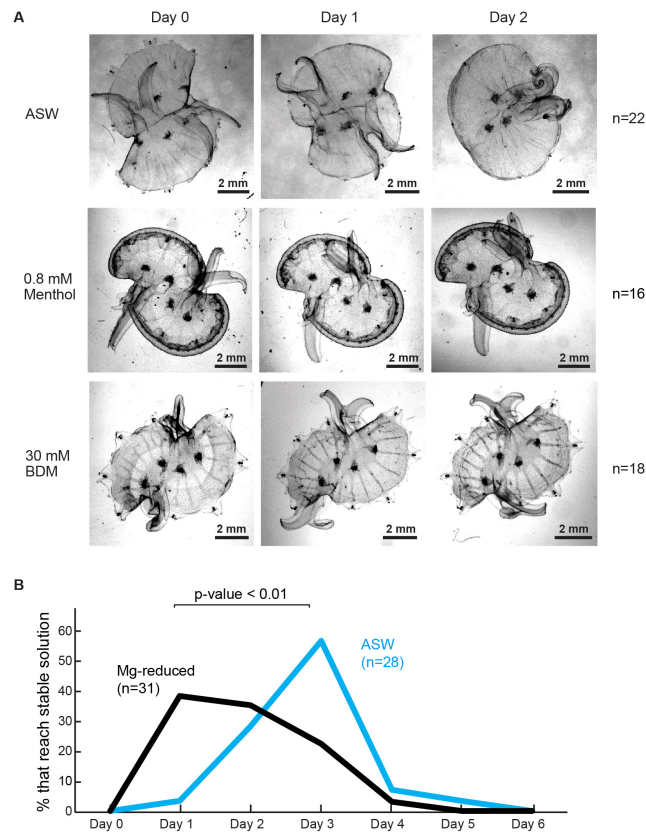
Figure 2.10: Modulating frequency of muscle contraction changes the rate of reorganization. A. Grafts incubated in 0.8mM menthol or 30 mM 2,3-butanedione monoxime (BDM) showed little reorganization over 2 days compared to those in control artificial seawater. Menthol is thought to inhibit pulsation by blocking voltage-gated ion channels that mediate the excitation-contraction coupling (Gaudioso et al., 2012), whereas BDM is a known inhibitor of muscle-specific type II myosin (Higuchi and Takemori, 1989). B. Conversely, increasing contraction frequency by placing the grafts in magnesium-reduced seawater increased the rate of reorganization. Magnesium is thought to modulate pulsation in marine invertebrates by acting on voltage-gated ion channels (Fawcett, Haxby, and Male, 1999). Grafts were checked daily for further reorganization. Data was collected over nine experiments.

2.6 *Aurelia* can sequentially reorganize body shape

Are these non-circular body shapes equilibrium solutions? Or are they stable because the processes driving reorganization stop after some point in time? If

Aurelia body shapes are truly dynamic equilibria, animals should not lose the ability to reorganize body shape after a stable shape has been found, and the same animal should be able to sequentially reorganize into different shapes. To test this, we allowed butterfly grafts to reorganize into rectangular animals, and then introduced additional geometric perturbations in the form of small notches to the sides of the chimera (Figure 2.11A). These animals readily reorganized into ovals. This suggests that reorganizational ability is not lost post-reorganization. However, as we introduced an additional injury prior to the second round of reorganization, this did not eliminate the possibility that *Aurelia* might initiate reorganization as a part of injury response.

If *Aurelia* shape reorganization is a dynamical system in which stable body shapes are dynamic equilibria, these equilibria might differ with different mechanical parameters. While we do not have the tools that would allow us to change parameters such as the material properties of the jellyfish body tissue, we were able to modulate the rate of muscle contractions. To test whether *Aurelia* might reorganize their shape in the absence of injury, we allowed offset grafts to reorganize into oval animals and tracked them over 2 weeks to ensure that the oval shapes reached stable states. We then placed the animals in reduced magnesium ASW to increase their rate of muscle contraction. After 2 more weeks, we measured the aspect ratio of these oval chimerae to check for further reorganization. We found that some of the animals reorganized into rounder solutions compared to oval animals that remained in ASW over 4 weeks (Figure 2.11B), which showed that injury is not required for shape reorganization. It also demonstrated that the capacity for reorganization does not disappear once a stable solution is achieved. This suggests that jellyfish shape is continuously regulated—not through muscle contractions that are induced by injury but rather the same contractions that propel *Aurelia* swimming during normal physiological function—and points toward a model of shape regulation where stable jellyfish shapes are dynamic equilibria of a mechanical dynamical system.

2.7 Discussion

Aurelia aurita are able to dramatically recover body shape post-development, and here we explored the mechanisms that drive shape recovery and whether they might regulate body shape in the absence of injury. Through grafting experiments, we found that not only can *Aurelia* mechanically recover radial symmetry in the event of injury, but that the same mechanism can also reorganize *Aurelia* shape in novel directions, generating stable oval, rectangular, trapezoidal, triangular, and asym-
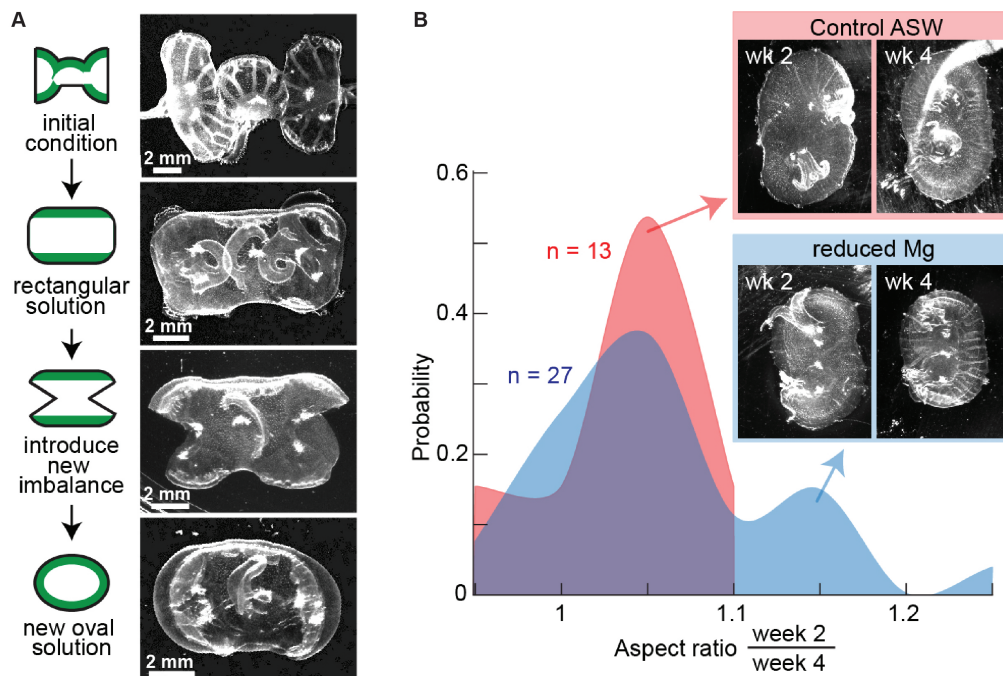
Figure 2.11: Grafted *Aurelia* can sequentially reorganize into different stable shapes. A. A butterfly graft was allowed to reorganize into a rectangular animal. Additional local geometric instabilities were introduced via notches cut into the short sides of the rectangle. The chimera proceeded to reorganize into an oval. B. Offset grafts were allowed to reorganize in ASW over 2 weeks into stable oval shapes. They were then placed into reduced magnesium ASW to increase their average contraction rate. Their aspect ratios were measured at 2 weeks and 4 weeks and compared to the aspect ratio at 2 weeks and 4 weeks of animals that stayed in ASW.

metrical jellyfish. The final shape produced by reorganization depends on the initial local geometry of the grafted jellyfish, suggesting that jellyfish shapes might be locally, rather than globally, regulated.

Interestingly, while radial symmetry has long been considered crucial to *Aurelia* swimming and feeding, many non-circular animals were still able to swim and feed and survived for over a month post-surgery. By visualizing the muscle through actin staining, we observed that the neighboring muscle bands reconnected, resulting in configurations that accommodated the non-circular jellyfish. The newly connected muscles also contracted synchronously, creating novel swimming behaviors in some non-circular animals that, while not as effective as the drawstring contractions of circular muscle bands, nevertheless allowed the animals to survive and grow. That circular muscle rings were not recovered and that local muscle reconfiguration was

sufficient for partial function recovery further support a locally-regulated model of shape reorganization.

Lastly, we found that individual *Aurelia* medusa are able to sequentially reorganize into multiple stable shapes. This additional shape change could be triggered by new injury or through an increase in muscle contraction rate. The latter suggests that shape reorganization is not simply an injury response. Instead, jellyfish shape might be continuously regulated during physiological function by swimming contractions, and that stable shapes are dynamic equilibria of a system of mechanical interactions.

While the flexibility and functional significance of body shape might be particular to Cnidarians, it is still possible that we may find parallel mechanisms for shape regulation throughout the animal kingdom. Even when body shape is defined skeletally, organs and tissues are viscoelastic and many experience regular mechanical forces. We hope our findings in *Aurelia* inspire the scientific community to imagine living shapes and structures as dynamic and to motivate more questions to be asked about how these shapes are regulated.

2.8 Supplementary Figures
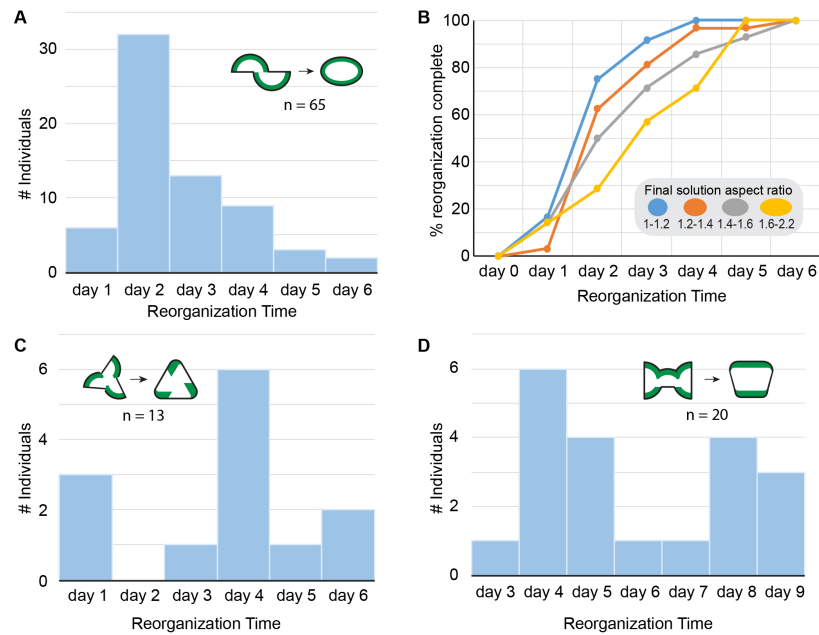
Figure 2.12: Reorganization time for different initial graft configurations. A. Offset graft reorganized into oval animals in 2.6 days on average (SD = 1.2 days). B. Offset grafts that reorganized into more elongated animals took longer to reorganize on average. C. Pinwheel grafts reorganized into round or triangular animals in 3.6 days on average (SD = 1.7 days). D. Butterfly grafts reorganized into rectangular or trapezoidal animals in 6.0 days on average (SD = 2.1 days).

A

Initial Condition | 2 weeks | 5 weeks

B

Initial Condition | 2 weeks | 4 weeks | 5 weeks

C

n = 13

Individual	1	2	3	4	5	6	7	8	9	10	11	12	13
C.V. (%)	4.5	6.2	4.3	4.2	4.6	4.2	4.2	4.0	5.0	5.3	6.9	3.3	3.5
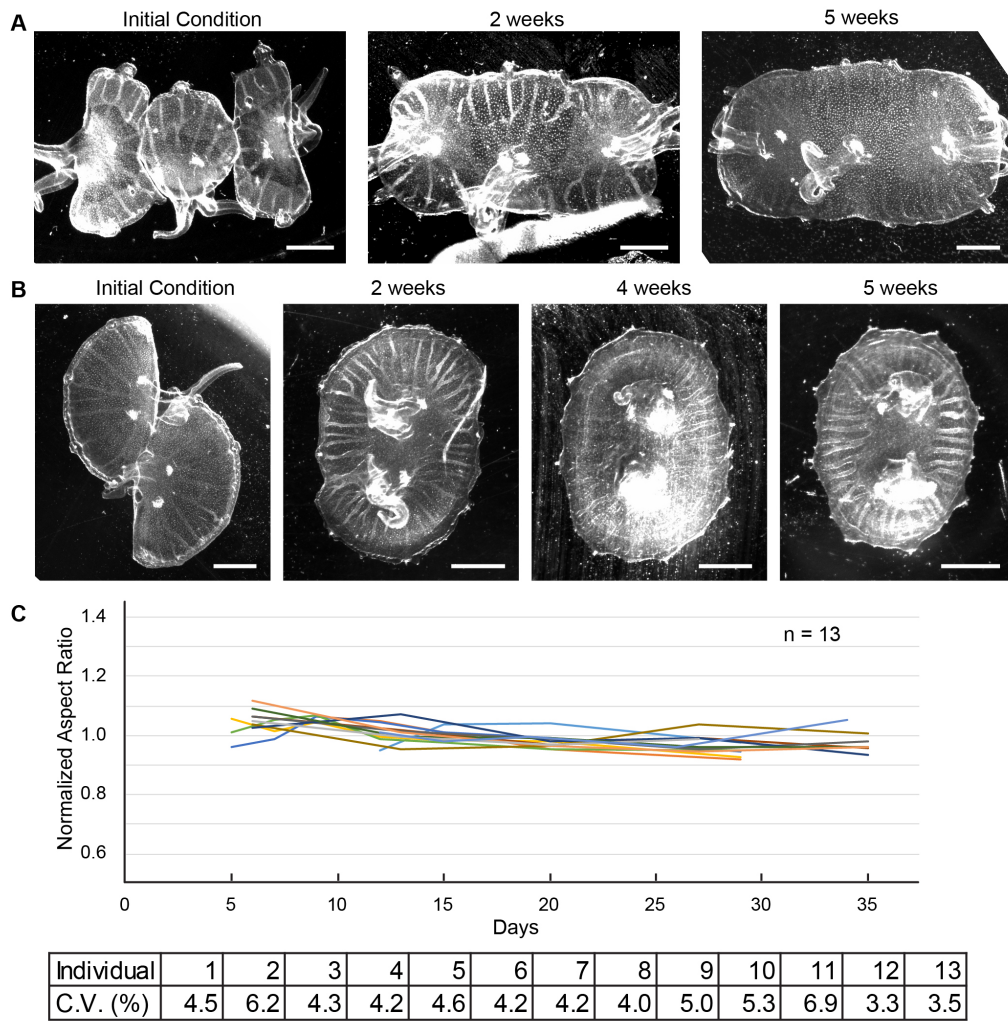
Figure 2.13: Novel jellyfish body shapes are stable. A. A butterfly graft and B. an offset graft completed reorganization within two weeks and maintained a stable shape when tracked over 3 more weeks. C. The aspect ratios of offset grafts (n=13) tracked for up to 30 days upon completion of reorganization showed negligible change over time.
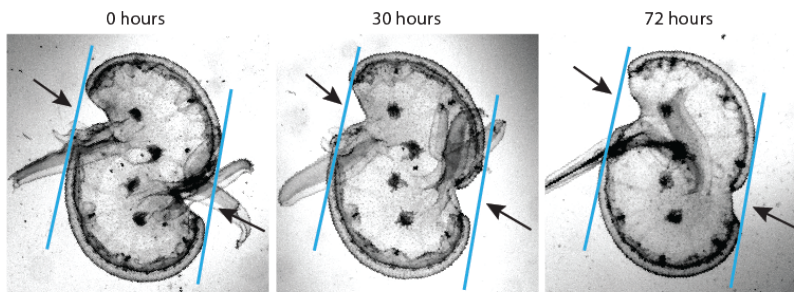
Figure 2.14: Some local smoothing occurs when muscle contraction is inhibited with menthol. The individual shown here is the same as in Figure 2.8A. An offset graft with muscle contraction blocked with 0.8mM menthol showed slow "filling in" of boundary concavities over three days (see black arrows), though no global reorganization occurs. The blue lines serve as references to help indicate the slow disappearance of the concavities.

2.9   Materials and Methods

Jellyfish culture. *Aurelia aurita* polyps were gifts from the Cabrillo Marine Aquarium (San Pedro, CA). Polyps were reared in artificial seawater (32 ppt ASW; Instant Ocean) at 72°F in recirculating box tanks with weekly water changes. Ephyrae and medusae were reared at 65°F in conic bubblers with daily water changes. The colony was fed daily with brine shrimp (*Artremia nauplii*) enriched with *Dunaliella salina* algae. Ephyrae were fed L-type rotifers (*Brachionus plicatilis*) for the first 3 days after strobilation, after which they were fed brine shrimp. Strobilation was induced chemically by incubating polyps in 25 µM 5-methoxy-2-methyl-indole (Sigma-Aldrich; M15451) overnight at 65°F, then returned to ASW, upon which strobilation typically occurred within 1 week (Fuchs et al., 2014). Strobilated ephyrae were grown to medusae in conic bubblers at 65°F. Conic bubblers are 5 gallon conical hatching jars (Pentair Aquatic Eco-systems; PART #: CCH1 to M100AP) with aeration from an air pump.

Grafting. *Aurelia aurita* medusae with empty gastric pouches 1-2 cm in diameter were anesthetized in 0.8mM menthol solution in ASW. A graft diagram with an outline for the desired shapes was placed under the dish to use as a template. Following the template, the medusa was then cut into the desired shapes using an Xact-O #17 chisel blade. The cut pieces were then immediately pinned in the desired configuration with their cut surfaces aligned to an agarose plate with cactus spines in menthol solution overnight. We found cactus spines from the *Espotoa* genus to be effective (e.g., *E. mirabilis* and *E. guentheri*). The agarose plates were prepared

with 1% SeaPlaque low melting point agarose in deionized water and wrapped with plastic wrap to avoid agarose dissolving into the menthol solution. Within 12-24 hours, the pieces fused together and were unpinned. The grafts were transferred to a petri dish with ASW and monitored for several weeks. Chimera were not fed during reorganization to avoid confounding effects from growth.

Modulation of muscle contraction frequency. Magnesium-free ASW was made using recipe 4 in table 3A in the Marine Biological Laboratory Recipe Book (*Biological Bulletin Compendia* 2017) and was mixed 1:3 with regular ASW to make magnesium-reduced seawater as used in experiments in Figure 2.10 and Figure 4.5. 0.8mM menthol (Sigma-Aldrich; M2772) solution in ASW was used as an anesthetic as well as a muscle inhibitor (Gaudioso et al., 2012). 30mM BDM (Sigma-Aldrich; B0753) solution in ASW was also used as a muscle inhibitor (Higuchi and Takemori, 1989). Muscle contraction frequency was measured using 10-second time-lapses videos of the animal on day 1 and day 4 after unpinning.

Muscle and neuron staining. Actin was stained using Alexa Fluor 488 Phalloidin (ThermoFisher Scientific; A12379) at 1:30 concentration. Neurons were stained with anti-tyrosinated-α-tubulin antibody (SigmaAldrich; T9028) and Alexa Fluor 594 goat anti-mouse IgG secondary antibody (ThermoFisher Scientific; A11005). Medusae were first anesthetized in 0.8mM menthol solution. They were then fixed in 4% formaldehyde in PBS for 1 hour, washed in PBS, permeabilized in 0.3% Triton X-100/PBS for 1 hour, blocked with 3% (vol/vol) NGS in 0.3% Triton X-100/PBS for 2 hours, and washed in 0.3% Triton X-100/PBS. For actin staining, medusae were then incubated in 1:30 phalloidin (in 0.3% Triton/PBS) overnight in the dark at 68°F, washed in 0.3% Triton/PBS, and imaged. For neuron staining, medusae were incubated in 3:2000 anti-α-tubulin antibody overnight at 4°C, repermeabilized in 0.3% Triton X-100/PBS for 2 hours, blocked in 3% (vol/vol) NGS in 0.3% Triton X-100/PBS for 1 hour, and incubated in 1:200 Alexa Fluor 594 anti-mouse secondary antibody in the dark overnight at 4°C. They were then washed in 0.3% Triton X-100/PBS and immediately imaged. For muscle/neuron costaining, medusae were incubated in 1:30 phalloidin solution overnight in the dark at room temperature after neuronal staining, and washed in 0.3% Triton X-100/PBS before imaging.

Microscopy and measurements of aspect ratio. Darkfield, brightfield, and fluorescent Aurelia were imaged using the Zeiss AxioZoom.V16 stereo zoom microscope and processed using the Zen software. Movies were captured using CamStudio

or using the Zen time series module. Aspect ratio was measured using the Zen software.

Quantification and statistical analysis. A two-tailed Welch's t-test was used to compare control and reduced-magnesium seawater jellyfish populations in muscle frequency experiments in Figure 2.10 (Ruxton, 2006).

References

Abrams, Michael et al. (2015). "Self-repairing symmetry in jellyfish through mechanically driven reorganization." In: *PNAS* 112, E3365–E3373.

Arai, Mary N. (1997). *A functional biology of Scyphozoa.* Chapman & Hall.

Bickell–Page, Louise R. and George O. Mackie (1991). "Tentacle autonomy in the hydromedusa *Aglantha digitale* (Cnidaria): an ultrastructural and neurophysiological analysis." In: *Philosophical Transactions of the Royal Society B* 331, pp. 155–170.

Biological Bulletin Compendia (2017). *Artificial Seawaters Recipes. Table 3a, Recipe 4.* Marine Biological Laboratory. URL: `comm.archive.mbl.edu/BiologicalBulletin/COMPENDIUM/CompTab3.html#3A` (visited on 04/2017).

Brusca, Richard and Gary Brusca (2003). *Invertebrates.* 2nd ed. Sinauer Associates.

Dabiri, John O. et al. (2005). "Vortex motion in the ocean: In situ viscualization of jellyfish swimming and feeding flows." In: *Physics of Fluids* 17, p. 91108.

Fawcett, William J., Elizabeth J. Haxby, and David A. Male (1999). "Magnesium: Physiology and pharmacology." In: *British Journal of Anaesthesia* 83, pp. 302–320.

Fuchs, Bjorn et al. (2014). "Regulation of polyp-to-jellyfish transition in *Aurelia aurita*." In: *Current Biology* 24, pp. 263–273.

Gaudioso, Christelle et al. (2012). "Menthol pain relief through cumulative inactivation of voltage–gated sodium channels." In: *Pain* 153, pp. 473–484.

Gemmell, Brad J. et al. (2013). "Passive energy recapture in jellyfish contributes to propulsive advantage over other metazoans." In: *PNAS* 110, pp. 17904–17909.

Gladfelter, William B. (1972). "Structure and function of the locomotory system of the Scyphomedusa *Cyanea capillata*." In: *Marine Biology* 14, pp. 150–160.

Higuchi, Hideo and Shigeru Takemori (1989). "Butanedione monoxime suppresses contraction and ATPase activity of rabbit skeletal muscle." In: *The Journal of Biochemistry* 105, pp. 638–643.

Norton, John H. et al. (1996). "An evaluation of some relaxants for use with pearl oysters." In: *Aquaculture* 144, pp. 39–52.

Ruxton, Graeme D. (2006). "The unequal variance t–test is an underused alternative to Student's t–test and the Mann–Whitney U test." In: *Behavioral Ecology* 17, pp. 688–690.

Chapter 3

DESIGNING A FINITE-ELEMENT MODEL OF *AURELIA* REORGANIZATION

3.1 Introduction

Moon jellyfish, *Aurelia aurita*, uses a mechanism of muscle contraction and viscoelastic response to regulate body shape. Through grafting experiments (described in Chapter 2 of this thesis), we observed that *Aurelia* medusa not only recover circular body shape from a wide variety of perturbations to body geometry, but can also reorganize their bodies into a range of novel body shapes. Our observations that animals achieved asymmetrical body shapes in addition to shapes with bilateral, radial, and rotational symmetry, suggested that body shape reorganization is regulated through local mechanical interactions, with little or no global feedback. Staining revealed that muscle reorganization, too, likely only occurs on a local level. Additionally, our findings that jellyfish can sequentially reorganize their shape indicates that jellyfish shape might be dynamic and continuously regulated. These results are in line with a model where jellyfish shape is a product of, and regulated by, mechanical self-organization.

To explore whether local mechanical forces and muscle reconnections are sufficient to explain jellyfish shape reorganization, we designed a finite element model to simulate the evolution of jellyfish shape during reorganization. Finite element models have been developed previously to simulate the large deformations involved in morphogenetic processes to test, for example, whether apical constriction could be responsible for movements such as *Drosophila* invagination and how cells might rearrange when an epithelial sheet is stretched (Conte, Muñoz, and Miodownik, 2008; H. Chen and Brodland, 2000; Brodland, D. Chen, and Veldhuis, 2006; Brodland and Clausi, 1994). While these studies have laid a foundation for how to apply finite element methods to biological materials and the dramatic shape changes they undergo, the applied stresses being tested in these models are relatively simple compared to those experienced by *Aurelia* during reorganization. During *Aurelia* reorganization, the primary driver of shape change, the muscle-generated force, is heavily dependent on the jellyfish geometry. We developed a formulation for calculating local muscle force from the jellyfish geometry such that the same

algorithm can be used to calculate muscle contraction force over the course of muscle reconnection without manual intervention. We also describe here a method for tracking the local viscoelastic stresses present within the jellyfish tissue over time. In conjunction, these form the foundation of our model of mechanical self-organization and allow us to test whether, and under what conditions, a system of mechanical self-organization could regulate jellyfish shape.

3.2 Modeling assumptions

Aurelia medusa have a saucer shaped bell. The bell is composed of two tissue layers—the epidermis and gastrodermis—and extracellular mesoglea, with mesoglea making up the bulk of the thickness of the bell. Mesoglea is a viscoelastic extracellular matrix that is 96-97% water and is comprised of collagen fibers, fibrillin homologues, as well as other structural proteins and polysaccharides (Gambini et al., 2012; Joshi et al., 2013; X. Wang, H. Wang, and Brown, 2011). In ephyra, the bell is thin with very little curvature. As the animals mature, the mesoglea layer increases in thickness more so at the center of the bell above the mouth and gastric pouches than at the periphery, resulting in increased bell curvature. Grafting was done in young *Aurelia* medusa with minimal bell curvature for ease of imaging, but which were large enough for ease of surgery. As a result, the animals were necessarily of an age where the bell thickness at the center of the bell was measurably greater than at the bell periphery (Figure 3.1).

The stiffness of mesoglea has been investigated in several studies previously. However, the Young's modulus of mesoglea reported varies widely between studies, from 60 Pa (equivalent to 20 Pa reported shear modulus by Gambini et al., 2012) to 30 kPa (Gambini et al., 2012; Joshi et al., 2013). Studies in *Aurelia* as well as *Rhopilema esculentum* and the hydromedusa *Polyorchis penicillatus* have found that stiffness can vary depending on whether forces are applied in tension or compression, in the radial direction or in the subumbrellar-exumbrellar direction, and on whole animals or isolated mesoglea samples (Megill, Gosline, and Blake, 2005; X. Wang, H. Wang, and Brown, 2011; Joshi et al., 2013). Even within a single study and single loading scheme, there was still variability in stiffness between individual animals. Due to the variability in reported material properties, we treat the stiffness and viscosity of jellyfish tissue as fit parameters.

There are other factors that contribute to the material properties of mesoglea, however. One is the matter of isotropy, or whether stiffness depends on directionality

of stress. Fibrous materials like mesoglea are in general stiffer in tension parallel to fiber orientation than perpendicular to fiber orientation and stiffer in tension than in compression (Fung, 1993). In *Aurelia*, scanning electron microscopy has revealed that both thick and fine fibers run throughout the mesoglea (Gambini et al., 2012). Thick fibers run vertically in the subumbrellar-exumbrellar direction and parallel to the exumbrellar surface in all directions. The fine fibers form a network that is randomly oriented and distributed. Within the plane of shape reorganization, that is in the radial and circumferential directions, there is no evidence in *Aurelia* that elastic fibers are oriented preferentially in any direction, and no studies of mesoglea viscoelastic properties have reported anisotropy between the radial and circumferential directions. As to whether the material behaves differently in tension versus in compression, Joshi et al. found that *Aurelia* mesoglea is 1–2 orders of magnitude stiffer in compression than in tension. However, compression tests were performed in the subumbrellar-exumbrellar direction and tension tests were performed in the plane of the bell, and differences in measured stiffness could also be due to these orientation differences. For the purposes of this model, we assume that jellyfish body tissue is isotropic and that material response to tensile and compressive stress are identical.
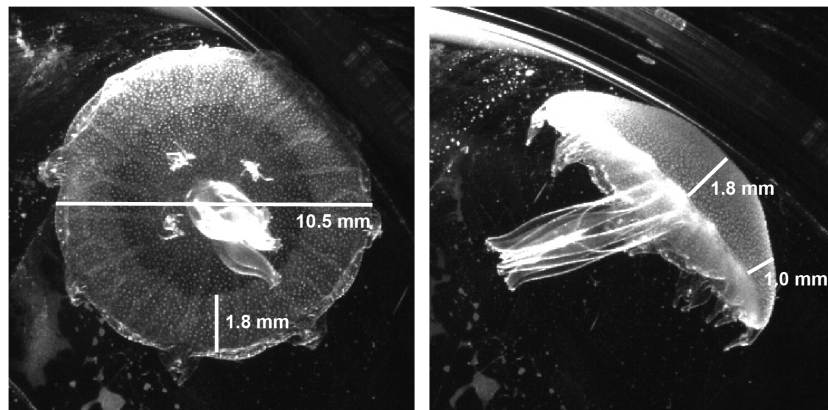
Figure 3.1: Dimensions of young *Aurelia* medusa. Left: Subumbrellar view of a young *Aurelia* medusa 10.5 mm in diameter, representative of those used in grafting experiments. The muscle ring, immature gonads, oral arms, and rhopalia can be seen. The estimated width of the muscle ring is 1.8 mm. Right: Lateral view of the same medusa. Measurements of bell thickness are shown at the center of the bell, above the mouth, and at the bell periphery above the muscle ring.

There is also the question of whether material properties are homogeneous throughout the medusa bell. As the center region of the bell near the mouth and gastric

pouches is thicker than the area around the periphery underlying the muscle ring, it would be reasonable to assume that the center of the bell might be stiffer than the periphery. Certain anatomical features might also differ in their material properties. For example, the area around the mouth, which has internal structures like the gastric pouches, might be stiffer and provide structural integrity or resistance to local shape reorganization, stabilizing the body shape of the jellyfish.

To test if there are structures within the jellyfish bell that provide additional stabilization for novel shapes, we excised the mouth and gastric pouches from *Aurelia* medusa and allowed them to heal, after which the bell was visually homogeneous. Removing the area of the bell surrounding the mouth also resulted in the removal of the thickest part of the bell. Once the bell healed, mouthless *Aurelia* were much more uniform in thickness across the whole bell compared to uncut animals. We performed offset grafts using the mouthless animals and found that the mouthless animals also reorganized into oval shapes (Figure 3.2A). The relationship between the offset distance of the initial graft geometry and the aspect ratio of the final oval body shape was similar to what was observed in regular offset grafts (Figure 3.2B). These results suggest that any structural support that might be provided by the mouth and gastric pouch or additional thickness at the center of the bell are not required for reorganization into stable oval shapes. For the purposes of this model, therefore, we assume that the bell material is homogeneous with no differences in stiffness due to jellyfish anatomy. We also assumed that the jellyfish bell was of uniform thickness.

Over the course of the <10 day time span of shape reorganization, grafted animals in our experiments were not fed (with the exception of the stability experiments) showing that feeding and increases in body mass were not necessary for reorganization. Over this time frame, we observed no growth in the chimera and no change in bell thickness. As Abrams et al. found that cell proliferation and apoptosis are not required for recovery of radial symmetry, the model assumes that the overall size of the jellyfish does not change during reorganization and that bell thickness does not change during reorganization. We also assumed that, since mesoglea is over 95% water, jellyfish body tissue is incompressible (Joshi et al., 2013). Additionally, we assume that the length of the muscle band does not change during reorganization. Although we observed some *de novo* muscle formation as the muscles formed connections across graft cut sites (Figure 2.8A), Abrams et al. showed that symmetry recovery proceeded even when actin polymerization is blocked, and that muscle growth is not required for shape reorganization.
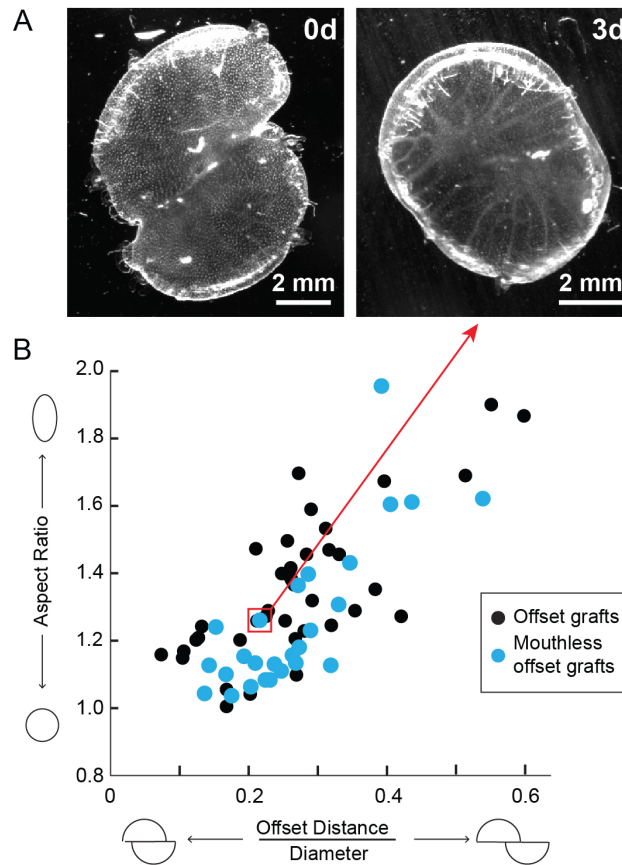
Figure 3.2: Mouthless offset grafts reorganized into ovals. A. Mouths were excised from young Aurelia medusa and the animals were allowed to heal. Once the cut site had fully healed such that the bell was visually homogeneous, the mouthless animals were grafted in an offset configuration. Images of a mouthless offset graft are shown immediately and 3 days after unpinning. B. Plot of offset ratio versus final aspect ratio in offset grafts without mouths (n = 29) plotted alongside data of offset grafts with mouths (n = 39).

Lastly, we assumed that muscle contractions occurred asynchronously and at regularly spaced intervals. In our experiments, we observed that muscle synchronization did not seem to affect the final stable shape of the animal. For example, we observed both asynchronous and synchronous contractions in the two muscle pieces that make up the bottom row of a stable trapezoidal chimera, depending on the animal. In offset grafts also, the final aspect ratio of the chimera did not depend on whether the muscle pieces had reconnected into an oval ring or had remained as two separate pieces as observed in S-shaped animals, or even had only connected on one side as seen in asymmetrical animals. As for the regularity of muscle contraction, although we did observe variation in the timing of contractions during our graft experiments,

the second-long scale of individual muscle contractions is so short compared to the days-long scale of reorganization that we assume that regularly spaced contractions at the average contraction rate are sufficient to capture the effect of contraction rate on reorganization.

In summary, we modeled the jellyfish body as an incompressible homogeneous isotropic material of uniform thickness acted on by regularly spaced periodic muscle contractions. The assumptions allow us to represent the jellyfish body in 2D and exclusively consider the forces acting within the 2D plane that drive shape change within that plane. They also allow us to focus on how our parameters of interest—contraction rate, contraction strength, stiffness, and viscosity—affect *Aurelia* shape reorganization.

3.3 Modeling equations and finite element implementation

Our goal in this model is to track the shape evolution of *Aurelia* medusa from the initial graft geometry as it undergoes mechanical force-driven reorganization. Because the extent of shape change during reorganization is quite dramatic, and because the forces acting on the jellyfish at any given point in time is dependent on the current shape of the jellyfish, we take an incremental approach where the net force at each time step is used to calculate local displacements and update the jellyfish shape, and that shape information is then used to calculate the net force acting on the jellyfish during the next time step (Figure 3.3).

The jellyfish geometry is discretized into a 2D mesh of triangular elements. The displacement of individual nodes is used to track the evolution of jellyfish shape over time, while edges act as viscoelastic trusses representing the tissue's material response. Depending on their location within the finite element mesh, nodes are classified as muscle, boundary, or bulk tissue. There are three forces acting on the jellyfish at any given time point: force from muscle contraction F_m, elastic force F_e, and pressure force F_p. The force from muscle contraction is treated as an external force that acts on the muscle nodes based on the geometry of the muscle piece. Elastic force acts on all nodes and is calculated based on the strain of the edges neighboring that node. Pressure force serves to maintain the incompressibility of the tissue and acts on boundary nodes depending on any change in volume of the jellyfish. The net force on any given node at time t is the sum of these three forces acting on that node:

$$F_{net}(t) = F_m(t) + F_e(t) + F_p(t).$$

The displacement of each node is then calculated at each time point as

$$\frac{dx}{dt} = \frac{F_{net}(t)}{\eta}$$

where η is the viscosity of the jellyfish body tissue. Due to the long timescale of shape reorganization, it is not necessary to take inertial forces into account (Brodland and Clausi, 1994; Odell et al., 1981).
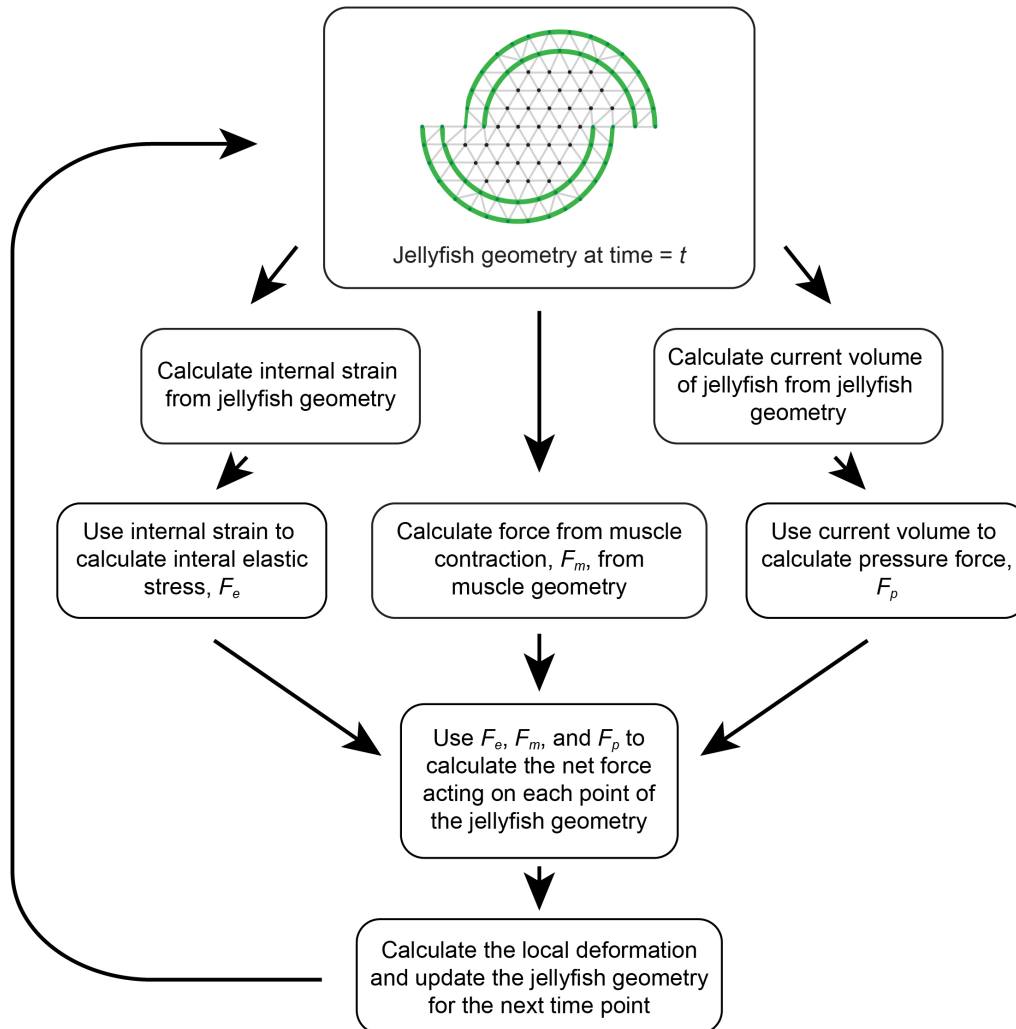

Figure 3.3: Model overview. The geometry of the finite element representation of jellyfish geometry is used at each time step to calculate the forces acting on each node during that time step. The net force acting on each node is then used to calculate the incremental displacement of each node, which is used to update the jellyfish geometry for the next time step.

Modeling muscle contractions

There are three components we took into consideration when modeling muscle contraction force: the direction, magnitude, and time dependency. We did not have a way to directly measure the force produced by muscles *in vivo* in our grafted animals. The model parameters we used to describe muscle contractions are therefore inferred from strain measurements during muscle contractions in grafted animals.

We observed in uncut *Aurelia* medusa that muscle contraction strains the bell in two directions: it shortens the muscle band in the circumferential direction and simultaneously contracts the subumbrella in the radial direction, bending the bell and increasing the bell curvature (Figure 3.4A). In conjunction, these two movements create the drawstring-like swimming contraction that squeezes water out of the subumbrella cavity and propels the animal forward (Gemmell et al., 2013; Arai, 1997). In uncut young *Aurelia* medusa such as used in the grafting experiments, the contraction is radially symmetrical: the muscle ring shortens uniformly along its length, resulting in a circular contracted muscle ring of decreased radius. In grafted animals with cut muscle pieces, however, that symmetry is broken. We observed that while the amount of circumferential shortening still seemed to be uniform along the muscle length, the radial compression depended on the local geometry of the graft. For example, when one end of a muscle piece is grafted into unmuscularized bulk tissue such as in the offset graft, the bulk tissue acts as an anchor that resists radial compression and bending of the bell. We observed in muscle pieces anchored at one end that the free end of the muscle tended to displace asymmetrically toward the anchored end, presumably due to increased resistance from the anchoring tissue. Radial compression and bending of the bell also occurred to a greater degree at the free end than at the anchored end.

To describe the direction of muscle contraction force mathematically in two dimensions, we decomposed the muscle force into radial and circumferential components (Figure 3.5A). We estimated the contracted geometry of each muscle piece by estimating the relative magnitude of these two components based on the geometry of the muscle piece and whether it was anchored at one, both, or neither end. We then define the direction of muscle contraction force at each muscle node to be the vector of displacement from its relaxed position to its respective contracted position.

The circumferential component of muscle contraction force was calculated using muscle contraction strain measured in offset grafts. The arc length of the muscle band was measured when fully relaxed and fully contracted, and the compressive
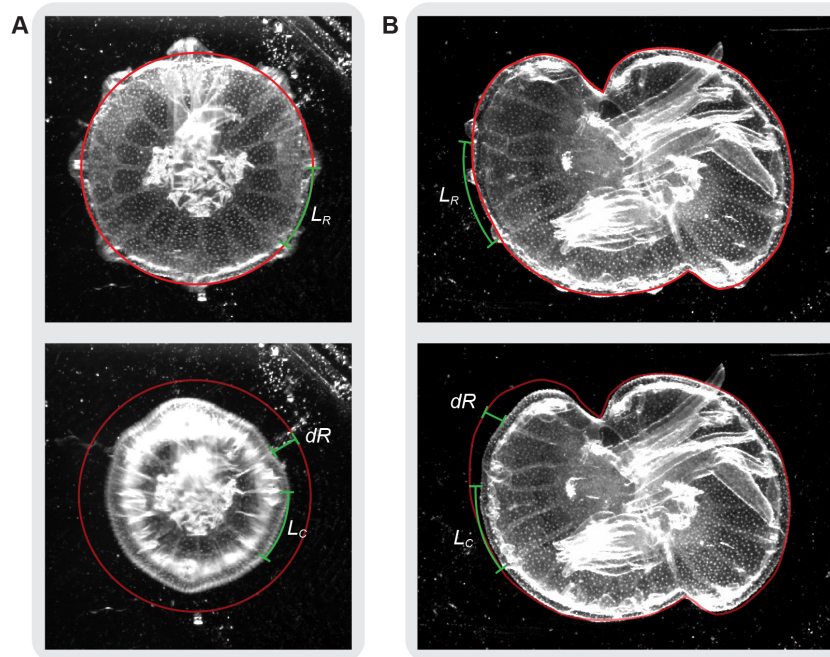
Figure 3.4: Geometry of muscle contraction in *Aurelia aurita*. A. Whole uncut *Aurelia* medusa in relaxed (upper) and contracted (lower) states in subumbrellar view. The muscle—labeled by L_R in the relaxed state and L_C in the contracted state, shortens circumferentially when contracted. The radius of the muscle ring decreases by dR as the bell curvature increases. B. One muscle piece (left) in an offset graft in its relaxed (upper) and contracted (lower) state, as viewed from the subumbrella. The muscle piece shortens circumferentially during contraction similarly to the uncut medusa. The relaxed half-medusa anchors one side of the contracting muscle, preventing it from bending out of the plane, causing dR to increase with distance from the anchoring piece.

strain ε_m was calculated as

$$\varepsilon_m = \frac{l_r - l_c}{l_r}$$

where l_r is the relaxed muscle length and l_c is the contracted muscle length. We found that the strain of muscle contraction ranged from 4% to 38%, with an average of 21% (SD = 7.6%, n=89) (Figure 3.6B). The direction of circumferential shortening was defined as toward the midpoint of the muscle piece with distance between relaxed nodes shortening by the same amount regardless of the position of the node along the muscle piece. This necessarily meant that nodes further away from the muscle midpoint experience a higher degree of circumferential displacement during contraction relative to radial displacement. Although asymmetry was observed in circumferential shortening of muscles in the offset graft, we encoded circumferential

shortening as symmetrical about the muscle midpoint, as the difference in observed displacement was likely a result of increased elastic resistance at the anchored end and not a result of asymmetrical force production from the muscle itself.

The radial component of the muscle force, however, was not modeled uniformly along the muscle length. Muscle that has been grafted onto unmuscularized bulk tissue is prevented from moving out of the plane of the bell by this bulk tissue and exerts less compressive force in the radial direction than muscle located further from these graft site. To calculate the radial component of muscle force, we first approximated the geometry of the muscle band as an arc. Since our experiments showed that mouths do not necessarily provide any unique structural support, the center point of each muscle arc was defined by the geometry of the muscle arc and not by the position of any neighboring mouths. The radius of the muscle arc was then defined as the average distance between the muscle band and its center point.

We estimated the radial strain using dR, the change in radius between the relaxed muscle piece and the contracted muscle piece, which increases linearly with distance away from any anchored muscle ends until some maximum dR, defined as the reduction in radius when no anchored ends are present. In muscles where neither end is anchored, or in the case of a fully connected muscle ring in oval and circular animals, every point on the muscle experiences the same radial compression. When one end is anchored, such as in the offset graft, the unanchored free muscle end experiences the greatest displacement in the radial direction during a contraction (Figure 3.5C). When both muscle ends are anchored, as in the butterfly graft, the midpoint is the furthest distance away from any anchored ends and experiences the greatest radial displacement (Figure 3.5D).

The estimated radial and circumferential displacement are used to calculate the estimated contracted geometry of each muscle piece, and the displacement vector between respective nodes in the relaxed and contracted muscle piece determine the direction of the muscle contraction force (Figure 3.5B, E, F). We found that varying the relative magnitudes of circumferential strain ε_m and radial strain dR can describe a wide range of possible muscle contraction behaviors. When $\frac{\varepsilon_m}{dR}$ is low, the arc angle of the muscle increases when contracted (Figure 3.5B), and when $\frac{\varepsilon_m}{dR}$ is high, the arc angle decreases when contracted. As there is natural variation in muscle contraction in our graft experiments, variation in this ratio might serve to explain how similar graft geometries could reorganize into rounded or polygonal shapes.
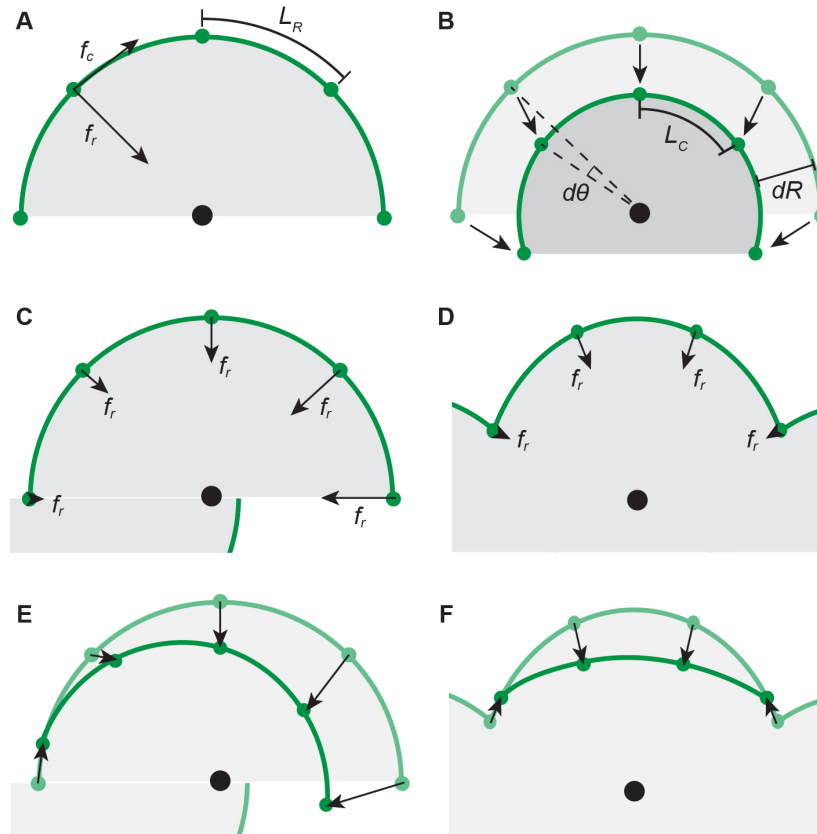
Figure 3.5: Calculations of muscle contraction force depends on muscle geometry. A. Muscle contraction force acting on each muscle node is calculated as a sum of radial force from the bending of the bell F_b and circumferential force from the shortening of the muscle band F_s. The calculation of F_b is dependent on the local geometry of muscle piece, while F_s is calculated in the same way regardless of geometry using a set contraction strain $\varepsilon = \frac{L_C - L_R}{L_R}$. L_R and L_C are the relaxed and contracted lengths of the muscle, respectively. B. Muscle force as calculated in an unanchored muscle piece such as a half medusa. F_s causes the muscles to contract to a length of L_c, and F_b causes a decrease in the radius of the muscle band by dR. These two forces in conjunction result in a net muscle force acting on each node (arrows) that results in the muscle's contracted geometry. Note that for small ε and large dR, the arc angle $d\theta$ of the muscle band increases when contracted, while arc angle decreases for large ε and small dR. C-D. The bending force F_b is small at anchored muscle ends and increases with distance from the anchored end, as unmuscularized bulk tissue is assumed to restrict neighboring muscle from bending. E. The net muscle force (arrows) and contracted geometry of a muscle piece anchored on one side. F. The net muscle force (arrows) and contracted geometry of a muscle piece anchored on both sides.

Once the direction of muscle contraction has been defined, the magnitude of muscle contraction force was calculated using the measured muscle strain and the stiffness of the mesoglea. Because muscle force was measured indirectly in grafted animals by measuring the strain, the muscle force required to recapitulate that strain is dependent on the viscoelastic properties of the body tissue. Mesoglea is predominantly elastic in its behavior on the second-long timescale of individual muscle contractions, so Hooke's Law was used to approximate the stress produced by the muscle:

$$\sigma = \lambda \varepsilon_m$$

where λ is the stiffness of the jellyfish tissue. Circumferential muscle strain was used to approximate the magnitude of muscle contraction force due to ease of measurement. Radial bending strain was not measured in the grafted animals.

Lastly, muscle force is not constantly active. Over any span of time, *Aurelia* medusa spend some fraction of time in a contracted state and the remaining time in a relaxed state. We used two parameters to mathematically describe the function of muscle force over time: contraction rate and contraction duration. In our grafting experiments, we found that contraction rate in young *Aurelia* medusa ranged from 3-66 contractions per minute and averaged 20 contractions per minute (SD = 12, n = 45). When muscle contraction rate was modulated by decreasing the magnesium concentration in the media, the contraction rate ranged from 9-77 contractions per minute and averaged 33 contractions per minute (SD = 16, n = 53).

To measure the duration of individual muscle contractions, we measured the time span between the initiation of muscle contraction and when the muscle band fully recovered its relaxed length using time-lapse images of offset grafts. We found that the length of a full contraction was on average 0.7 seconds, (SD = 0.1s, n=118) and that this duration was very consistent at low contraction rates (Figure 3.6A). However, at high contraction rates, the average duration of a contraction decreased slightly. We observed that in very active animals, contractions would occasionally initiate before the muscles had fully relaxed, effectively interrupting the previous contraction and cutting it short. As contraction rate increased, these interrupted contractions occured more often, decreasing the average duration of individual contractions. For the purposes of the simulation, we set contraction duration t_c as 0.8s. The contraction duration, in conjunction with contraction rate, was used to find the average length of time spent at rest between contractions. In an animal with contraction rate of n contractions per minute, the length of the rest phase t_r between

contractions is

$$t_r = \frac{60 - nt_c}{n}.$$

.

In our simulations, muscle force is only applied for the duration of t_c. For the duration of the rest phase, the muscle force is set to zero and the net force is equal to the sum of the elastic force and pressure force.
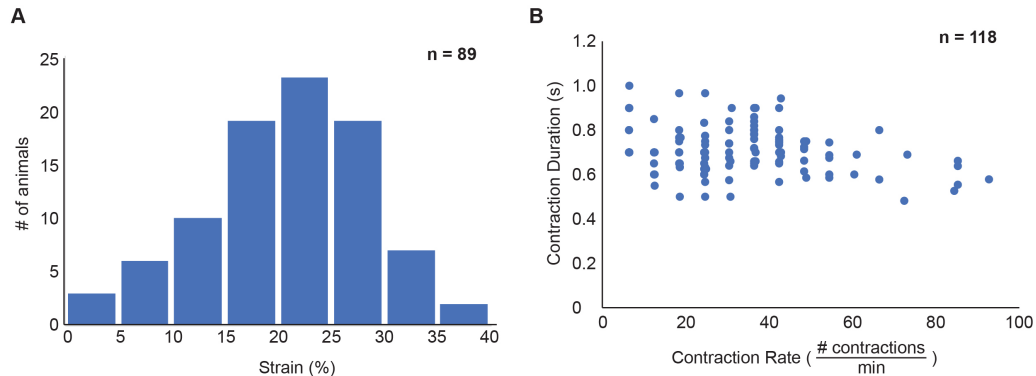
Figure 3.6: Measurements of muscle contractions in *Aurelia* grafts. A. During muscle contraction, muscle bands in offset grafts shorten on average by 21%, with a range of strains between 4% and 38%. (SD = 7.6%, n = 89). B. While for the most part contraction duration in offset grafts is constant regardless of contraction rate, as contraction rate increases, the chance that contractions initiate before muscles fully relax increases, effectively interrupting the previous contraction and reducing the average time spent during each contraction phase. The average contraction duration is 0.7 seconds. (SD = 0.1 s, n = 118)

Material properties of *Aurelia aurita*

The mesoglea of *Aurelia aurita*, which makes up the bulk of the bell tissue, is a viscoelastic extracellular matrix and an important component of *Aurelia*'s propulsion machinery. After muscle contractions, the mesoglea elastically recoils, pulling the muscle back to its relaxed length, which suggests that mesoglea is dominated by elastic behavior at the timescale of individual muscle contractions (Gemmell et al., 2013). At the same time, our experimental results indicate that *Aurelia* body tissue is capable of permanent deformation as the animals are able to reorganize their shape into a new stable shape. Thus, on the time scale of shape reorganization, the tissue displays a large degree of viscous dissipation. This mix of elastic, solid-like behavior on short timescales and viscous, liquid-like behavior on long timescales is characteristic of viscoelastic materials. The timescale at which a material switches from being primarily elastic to primarily viscous is called the relaxation time. All biological materials are viscoelastic to some degree, but can usually be modeled as purely viscous or purely elastic depending on the timescale of the forces or processes of interest (Fung, 1993; Brodland and Clausi, 1994; H. Chen and Brodland, 2000; Brodland, D. Chen, and Veldhuis, 2006; Savin et al., 2011). In *Aurelia*, however, we are both interested in both second-scale muscle contractions and days-long shape reorganization, so aimed to model the jellyfish tissue in a way that can capture both viscous and elastic behaviors.

Viscoelastic materials are modeled as combinations of elastic and viscous elements: springs and dashpots (Vogel, 2004; Fung, 1993). The spring stores elastic stress and recoils when that stress is removed. The dashpot dissipates elastic stress and allows the material to irreversibly deform. By placing these elements in series and parallel, we are able to capture a wide range of viscoelastic behaviors. The simplest of these models are the Maxwell model—a spring and dashpot in series—and the Kelvin-Voigt model—a spring and dashpot in parallel. Maxwell materials are quite fluid and continuously deform under constant stress. Materials modeled this way would likely reorganize, but perhaps not find a stable state. In contrast, Kelvin-Voigt materials reach an equilibrium strain under constant stress, but will recoil to their unstressed shape when that stress is removed. A material modeled this way is unlikely to display dramatic shape change. As jellyfish tissue likely lies somewhere between these two extremes, we chose to model it as a standard linear material, composed of a spring in parallel with a Maxwell element (Figure 3.7). Tuning the stiffnesses of the two springs in a Standard Linear Model allowed us to capture a range of behaviors that includes those of the Maxwell and Kelvin-Voigt models. We

fit these two stiffnesses, along with the viscosity, to capture the shape reorganizing behavior of *Aurelia aurita*.
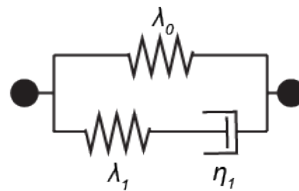

Figure 3.7: The Standard Linear Model of viscoelasticity consists of a spring in parallel to a Maxwell element. λ_0 and λ_1 are the stiffnesses of the springs. η_1 is the viscosity of the dashpot.

Viscoelastic properties are implemented in our finite element model by treating each of the edges between nodes as a standard linear material. While there exists a constitutive equation for the Standard Linear Model that relates stress, stress rate, strain, and strain rate, the stress present in the *Aurelia* tissue at any given time is dependent on the geometry at that time. We therefore chose to track the strain of the two springs and used these strains to calculate the elastic stress present in the system at any given time. This meant that the elastic force F_e acting along the *i*-th edge is calculated using Hooke's Law for two springs in parallel as

$$F_{e,i}(t) = -(\lambda_0 \varepsilon_0(t) + \lambda_1 \varepsilon_1(t))$$

where ε_0 and ε_1 are the strains of the two springs.

ε_0, the strain on the spring in parallel, was found with a simple calculation based on the relaxed length of the edge and the current length of the edge:

$$\varepsilon_0(t) = \frac{l(t) - l_0}{l_0}.$$

The strain on the second spring, ε_1, however, decreases over time as it is part of a Maxwell element and the dashpot allows for dissipation of stress and permanent deformation. We implemented this by treating the displacement of nodes at each time step as a constant strain and allowing the Maxwell element to relax for the duration of each time increment. We could then calculate the new relaxed length of the spring at time t using the relaxation equation for a Maxwell material under constant strain.

$$\varepsilon_1(t) = \varepsilon_1(t-1)e^{\left(-\frac{\lambda_1}{\eta}dt\right)}$$

where $\varepsilon_1(t-1)$ is the strain on the Maxwell element at the previous timepoint

$$\varepsilon_1(t-1) = \frac{l(t) - l_0(t-1)}{l_0(t-1)}.$$

The new relaxed length of the Maxwell element is therefore

$$l_0(t) = \frac{l(t-1)}{\frac{l(t)-l_0(t-1)}{l_0(t-1)}e^{-(\frac{\lambda_1}{\eta}t_r)} + 1}$$

and is used to calculate the strain of the spring at time t, $\varepsilon_1(t)$:

$$\varepsilon_1(t) = \frac{l(t) - l_0(t)}{l_0(t)}.$$

The elastic force of all k edges connected to each node contribute to the net elastic force acting on each node:

$$F_e(t) = \sum_{i=1}^{k} F_{e,i}(t).$$

In addition to an elastic force, we applied a pressure force to maintain the incompressibility of the jellyfish tissue. To allow for flow of material between finite elements, we did not calculate change in volume of individual elements, but rather considered the volume of the animal as a whole and applied this pressure force only to nodes on the boundary. As we assume that the thickness of the tissue does not change during reorganization, the volume was estimated using the total area of the jellyfish geometry calculated via this classic equation:

$$A = \frac{1}{2}((x_1y_2 + x_2y_3 + ... + x_ny_1) - (x_2y_1 + x_3y_2 + ... + y_nx_1)).$$

The pressure force F_p at time t acting on each boundary edge was calculated as

$$F_{p,i}(t) = -\frac{A(t) - A_0}{A_0}k_b$$

where k_b is the bulk modulus of jellyfish tissue. As the length of edges in the finite element mesh are maintained at around 1, we assumed that pressure force acted on all boundary surfaces equally. The pressure force acting on each boundary node was then defined as the sum of the pressure forces acting on its neighboring edges.

Finite element representation of jellyfish geometry

The jellyfish geometry was represented by a mesh of triangular elements. Each vertex in the mesh was tracked as a finite element node. The edges are treated as viscoelastic trusses that provide elastic resistance and viscous dissipation. All edges in the jellyfish mesh have the same viscoelastic properties, while nodes are designated as bulk tissue, muscle, or boundary.

In *Aurelia* medusae, circumferential muscle is embedded in a flat ring within the subumbrellar epidermis extending from the bell periphery inward. The muscle ring is narrow in ephyrae and increases in width toward the bell center as the animals mature. In young *Aurelia* medusa as used in our grafting experiments, the muscle band width was around 30% of the bell radius. We therefore designated the outer two rings of nodes as muscle nodes to approximate this geometry (Figure 3.8). Muscle force was treated as an external force that applies exclusively to muscle nodes. We defined outer and inner muscle separately, with inner muscle experiencing half of the magnitude of muscle force as the outer muscle as to provide some stability during simulations. Pressure force is applied to boundary nodes, defined as the nodes that line the periphery of the jellyfish mesh. All nodes are also designated as bulk tissue, and are acted on by elastic force from neighboring edges.

To create finite-element representation of our graft geometries, the mesh of the whole *Aurelia* medusa was cut and rearranged in the same manner as during grafting experiments. The offset graft geometry was created using two semicircular meshes "grafted" together at the desired offset distance (Figure 3.9A). The butterfly graft geometry was created with two semicircular meshes "grafted" to and connected by a small trapezoidal mesh (Figure 3.9B). The position of nodes at the boundary between grafted pieces was determined by averaging the position of node in each piece that most closely neighbored each other. Nodes at exposed cut edges were defined as boundary nodes. Additional edges were added to define the boundary as needed. The jellyfish mesh was updated periodically when certain conditions were met to maintain the stability of model calculations, to simulate the continuous and self-healing nature of the jellyfish material and to maintain the length of the muscle band throughout shape reorganization. There were three conditions under which the jellyfish mesh was updated in order to maintain homogeneous coverage of the jellyfish geometry and maintain stability of calculations. First, short edge lengths made it more likely that the connected nodes might cross each other before the next time increment and create instabilities in the calculations. To avoid this, when the
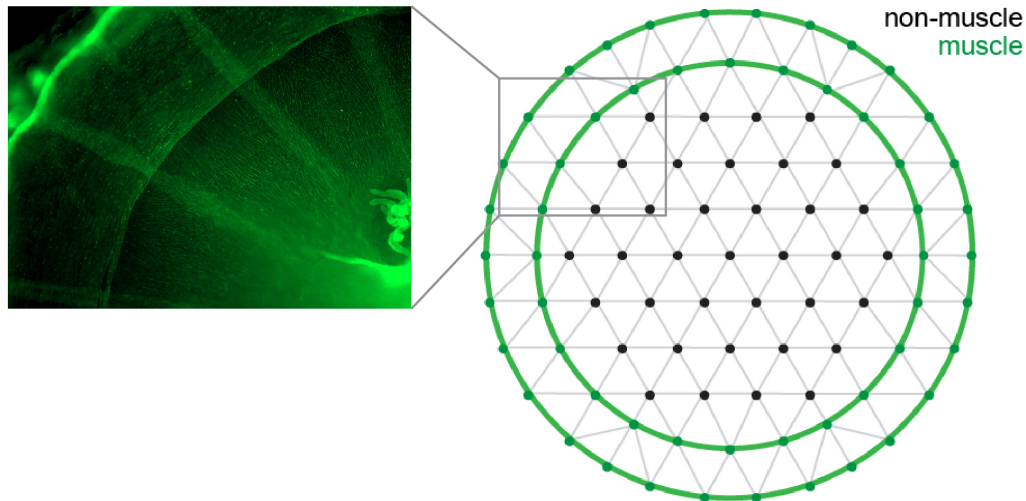
Figure 3.8: Finite element decomposition of uncut *Aurelia* medusa. Medusa were decomposed into triangular elements. The muscle band is represented by two rings of nodes (green) that run parallel to the edge of the mesh geometry. Unmuscularized bulk tissue is represented by black nodes.
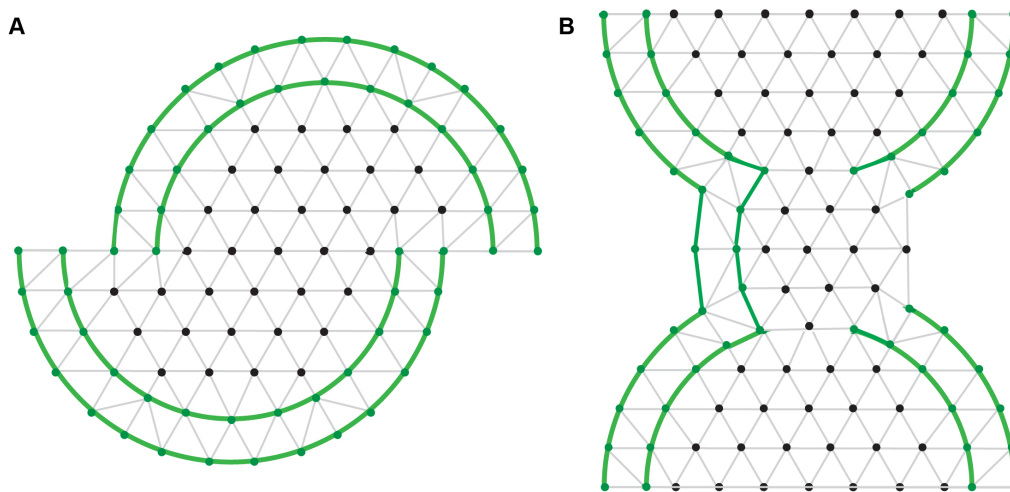
Figure 3.9: Finite element decomposition of jellyfish graft geometry. A. Finite element mesh of an offset graft with offset ratio of 0.2. Muscle nodes are demarcated in green. B. Finite element mesh of a butterfly graft. Muscle nodes are demarcated in green.

distance between two connected "parent" nodes fell below a certain threshold, the two parent nodes would be replaced by a single "offspring" node that connected to all nodes previously connected to either of the parent nodes. These new edges would also inherit the strains from the previous edges to maintain material integrity

(Figure 3.10A). Second, if the distance between two connected nodes exceeded a certain threshold, a new offspring node would be created at the midpoint of the edge connecting the parent nodes. The offspring node would be connected to the parent nodes as well as every node that is connected to both parents (Figure 3.10B). This helped to maintain homogeneity in the jellyfish mesh and prevent the creation of gaps that would not provide adequate viscoelastic response. Third, in the case that a triangular element became extremely elongated such that the length of one edge was a significant fraction of the combined lengths of the other two edges, the first edges was replaced by a perpendicular edge when possible (Figure 3.10C). This also served to maintain homogeneity in the jellyfish mesh by preventing two edges from providing viscoelastic response in the same direction in a very small area.

The jellyfish mesh was also updated periodically to simulate the self-healing properties we observed in *Aurelia*. When the distance between boundary nodes n and $n + 2$ fell below a certain threshold, a new edge was created to connect them, and boundary node $n + 1$ was no longer defined as a boundary node (Figure 3.10D). This was necessary to recapitulate what we observed in the offset grafts, that the perimeter of the initial graft geometry was often greater than the perimeter of the oval jellyfish post-reorganization. Specifically, the straight edges of the offset graft geometry shifted to the interior of the animal during reorganization, resulting in the convergence of the mouths and reorganization of the muscle piece into a connected oval muscle ring.

Lastly, the jellyfish mesh was updated to maintain the overall length of the muscle. Because the jellyfish body tissue is one continuous material with no compartmentalization, finite elements do not represent fixed points in the jellyfish tissue. Change in length of the muscle band as defined by the jellyfish mesh might therefore not be representative of actual shortening of the muscle band during reorganization. In fact, we observed in our grafts that muscle bands do not shorten significantly during the days-long reorganization process. To maintain the muscle band during simulations, the total muscle length is tracked, and if it falls below a certain threshold, additional nodes on either end of muscle pieces are assigned as muscle nodes during remeshing until the length threshold is met.

Simulation

Aurelia medusa are under constant elastic stress. This can be observed when a cut is made in a medusa bell and the cut immediately widens as the stress is released.

To create this internal stress in our model, we set the relaxed area artificially high at 0.1% greater than the calculated jellyfish mesh area, creating a positive pressure outward. The jellyfish mesh is then allowed to come to equilibrium, with elastic stress acting against the pressure force of the mesh. Thus, before the simulation starts, there is already elastic stress in the jellyfish tissue.

During the simulation, the geometry of the jellyfish mesh at time t is used to calculate the muscle force, elastic force, and pressure force at time t. Because muscle force is only active when the jellyfish is contracted and the jellyfish only spends a fraction of time in a contracted state, the average net force acting on each node during each time increment is calculated as

$$F_{net}(t) = (F_m(t) + F_e(t) + F_p(t))t_c + (F_e(t) + F_p(t))t_r$$

where t_c and t_r are the time the jellyfish spends contracted and relaxed during each time increment respectively. This net force is used to calculate the displacement of the nodes at time t, and the jellyfish geometry is updated. The viscoelastic material is also allowed to relax and relaxed lengths and strains are updated for the next time increment. Time increments of 15-30 minutes were used during simulations as there was no observable reorganization in our grafts within this time frame.
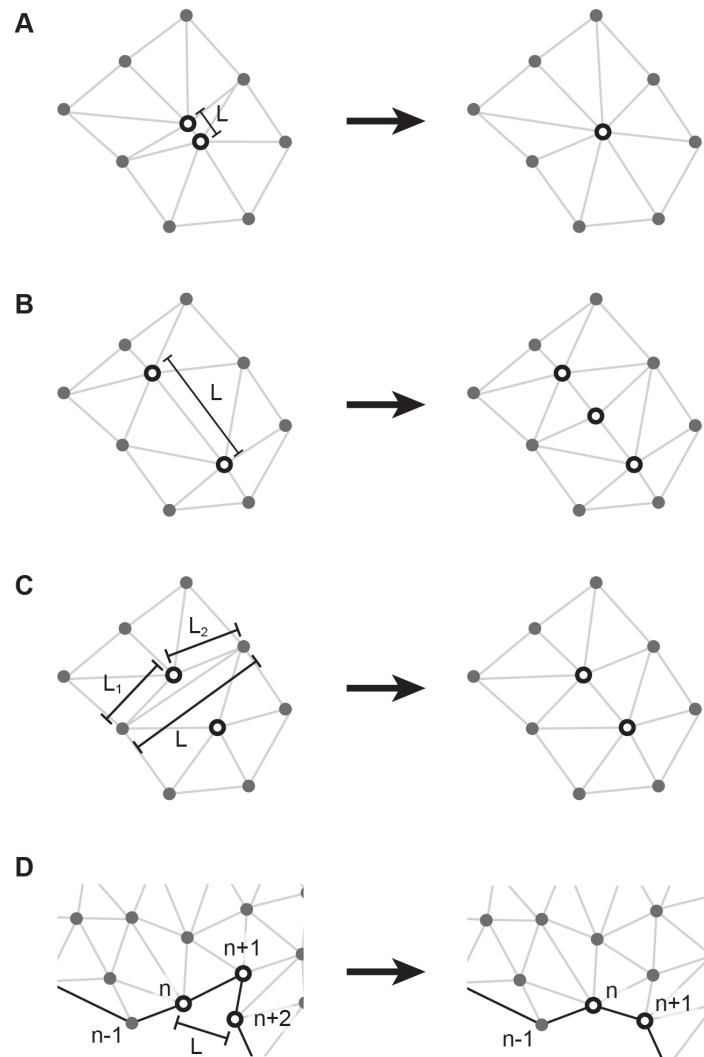
Figure 3.10: The jellyfish mesh was updated periodically during reorganization if certain conditions are met. A. When the length of an edge, L, falls below a certain threshold, the two parent nodes connected by that edge are replaced by a single offspring node to maintain stability of model calculations. The offspring node is connected to all neighboring nodes of the parent nodes. B. When the length of an edge, L, becomes greater than a certain threshold, a new node is added at the midpoint of that edge to maintain even mesh coverage of the geometry. The new node is connected to the parent nodes, as well as any neighboring nodes shared by the parents. C. When a finite element becomes elongated such that L is a significant fraction of $L_1 + L_2$, the edge with length L is replaced (when geometry allows) by a perpendicular edge to maintain even mesh coverage of the geometry. D. When the distance between two boundary nodes, n and $n + 2$, falls below a certain threshold, a boundary edge is added connecting the two nodes to simulate the self-healing properties of jellyfish tissue. The previous boundary node $n + 1$ is no longer considered on the boundary.

The jellyfish mesh was updated when the previously discussed conditions were met to maintain the total length of the muscle pieces, allow the material to self-heal, and maintain the homogeneity of the jellyfish mesh. Aspect ratio of the simulated offset graft was calculated in the same was as in our experiments: the major axis was defined as the diameter of the circle that circumscribed the jellyfish mesh and the minor axis was defined as the width of the jellyfish mesh perpendicular to the major axis. Reorganization into stable oval shapes in the offset graft was used to fit the stiffness, viscosity, muscle strain, and *dR* parameters.

3.4 Discussion

There were two major challenges in modeling *Aurelia* reorganization. The first was that there were two vastly different timescales at play: second-scale for muscle contractions and day-scale for reorganization. Since jellyfish tissue is viscoelastic, the material response to forces at each time scale are dramatically different. We addressed this issue by treating the body tissue as purely elastic when calculating the muscle forces from the measured muscle strain while allowing the tissue to undergo viscous relaxation over the course of each time increments for the purposes of calculating stored elastic stress. The second challenge was that the forces acting on the jellyfish during reorganization are dependent on the current geometric state of the system and thus, nonlinear. While an incremental approach to finite element modeling has been used in modeling morphogenetic processes before, the strategy has primarily served to accommodate the large deformations rather than to calculate active forces (H. Chen and Brodland, 2000). Modeling muscle forces in *Aurelia* required us to create a set of rules by which the muscle contraction force at each time point could be calculated consistently, without manual intervention, and that could be generalized across grafting schemes. We designed an algorithm where muscle force was characterized by two variables that could be calculated automatically using the mesh geometry, and this allowed us to isolate the changes to reorganization that were caused by different initial geometry.

We designed this model to be the simplest possible approximation of the forces present in *Aurelia* that could still recapitulate shape reorganization. The jellyfish bell and forces therein are represented in two dimensions, the tissue is treated as isotropic and homogeneous, and cellular processes are excluded altogether. The finite element mesh used is also coarse-grained to reduce computational demand. However, we found such a coarse-grained mesh sufficient to approximate the evolution of jellyfish geometry during reorganization.

This model was elaborate enough to allow us to explore the parameter space and assess what material properties might be required for shape reorganization while at the same time being simple enough that simulation results could be intuitively understood. However, the lack of consistent measurements of mesoglea material properties and our inability to directly measure muscle force limits the predictive ability of our simulations. Future characterizations of jellyfish mesoglea and muscle contraction force might allow us to concretely predict the material parameters that would allow for shape reorganization and inspire the design of synthetic, shape-changing materials.

References

Arai, Mary N. (1997). *A functional biology of Scyphozoa.* Chapman & Hall.

Brodland, G. Wayne, Daniel Chen, and Jim H. Veldhuis (2006). "A cell-based constitutive model for embryonic epithelia and other planar aggregates of biological cells." In: *International Journal of Plasticity* 22, pp. 965–995.

Brodland, G. Wayne and David A. Clausi (1994). "Embryonic tissue morphogenesis modeled by FEM." In: *Journal of Biomechanical Engineering* 116, pp. 146–155.

Chen, Helen and G. Wayne Brodland (2000). "Cell-level finite element studies of viscous cells in planar aggregates." In: *Journal of Biomedical Engineering* 122, pp. 394–401.

Conte, Vito, José Muñoz, and Mark Miodownik (2008). "A 3D finite element model of ventral furrow invagination in the Drosophila melanogaster embryo." In: *Journal of the Mechanical Behavior of Biomedical Materials* 1, pp. 188–198.

Fung, Yuan–Cheng (1993). *Biomechanics: Mechanical properties of living tissues.* Springer, New York.

Gambini, Camille et al. (2012). "Micro- and macrorheology of jellyfish extracellular matrix." In: *Biophysical Journal* 102, pp. 1–9.

Gemmell, Brad J. et al. (2013). "Passive energy recapture in jellyfish contributes to propulsive advantage over other metazoans." In: *PNAS* 110, pp. 17904–17909.

Joshi, Keyur et al. (2013). "*Aurelia aurita* inspired artificial mesoglea." In: *Integrated Ferroelectrics* 148, pp. 53–66.

Megill, William M., John M. Gosline, and Robert W. Blake (2005). "The modulus of elasticity of fibrillin–containing elastic fibres in the mesoglea of the hydromedusa *Polyorchis penicillatus*." In: *Journal of Experimental Biology* 208, pp. 3819–3834.

Odell, Garrett M. et al. (1981). "The mechanical basis of morphogenesis: I. Epithelial folding and invagination." In: *Developmental Biology* 85, pp. 446–462.

Savin, Thierry et al. (2011). "On the growth and form of the gut." In: *Nature* 476, pp. 57–62.

Vogel, Steven (2004). *Comparative Biomechanics: Life's physical world.* 1st ed. Princeton University Press.

Wang, Xuezhen, Huiliang Wang, and Hugh R. Brown (2011). "Jellyfish gel and its hybrid hydrogels with high mechanical strength." In: *Soft Matter* 7, p. 211.

AURELIA SHAPE DYNAMICS ARE REGULATED BY MECHANICAL SELF-ORGANIZATION

Modeling is an invaluable tool in studying the role of mechanical interactions during morphogenesis. Unlike with genetic and chemical interactions, there is not a suite of tools that can be used to easily activate, tune, or inhibit mechanical interactions *in vivo*. Tools have been developed for measuring mechanical forces and stresses in cells and tissues, but these tools do not identify the producer of these forces or whether these forces are responsible for driving morphogenesis (Sugimura, Lenne, and Graner, 2016). Modeling allows us to test hypotheses relating the forces present in and the material properties of living cells and tissues to the evolution of morphogenetic shape of these tissues over time (Brodland, 2015).

In this chapter, we describe the simulation results of the model of self-organization-driven shape change developed in Chapter 3. We ask whether a system of mechanical self-organization can recapitulate the kind of shape change we observe in our grafting experiments in the absence of global feedback and cellular processes. We also explore whether shape stability can really be reached if the mechanical forces that drive shape reorganization are still present post-organization. We investigate whether the same mechanical processes can produce multiple stable non-circular solutions. Lastly, we query the parameter space to understand how muscle force, stiffness, and viscosity affect the rate of reorganization and final jellyfish shape.

4.1 Local mechanical forces were sufficient to recapitulate reorganization of jellyfish into new stable body shapes

Are local interactions between muscle contraction force and viscoelastic response sufficient for reorganization? We initially modeled the viscoelastic properties of jellyfish body tissue as a standard linear material where the stiffnesses of the two springs, λ_0 and λ_1, were equal. Simulations of the offset graft under this paradigm did indeed reorganize to some extent, but they did not fully reorganize into ovals in which the concavity at the graft site fully disappeared as they did in our offset graft experiments (Figure 4.1B). When we decreased the ratio of λ_0 to λ_1 to 1:4, simulated offset grafts did fully reorganize into oval shapes even though the short term stiffness of the material, $\lambda_0 + \lambda_1$, remained the same (Figure 4.1A). When we increased the

ratio of λ_0 to λ_1 even further to 4:1, we observed even less reorganization in simulated offset grafts (Figure 4.1C). This was especially apparent in offset grafts with higher offset distances, in which reorganization stopped even when there was considerable concavity remaining. This result is not unexpected: when the ratio of λ_0 to λ_1 is high, a standard linear material behaves more akin to a Kelvin-Voigt material and is effectively more solid and less prone to irreversible deformation, which is required for shape reorganization. On the other hand, a standard linear material with a low λ_0 to λ_1 ratio behaves more similarly to a Maxwell material and is more fluid. We would expect such a material to more readily change shape, but also to be less likely to produce stable, non-circular shapes.

Surprisingly, in certain parameter paradigms, we found that simulated offset grafts did reorganize into stable oval shapes (Figure 4.2). One parameter that affected the model's ability to reorganize into a stable state was relaxation time, which is defined as

$$\tau = \frac{\eta}{\lambda_1}$$

in a standard linear material. We found that offset simulations with relaxation time between 3.5-11.6 hours reached 80% of the final aspect ratio between 200-500 hours of simulation time and fully reorganized into stable oval shapes within 700 hours of simulation time. In comparison, offset graft experiments visually completed reorganization between 24-96 hours, although the aspect ratio continued to display minor fluctuations over 840 hours of tracking (Figure 2.11B). Parameter sets where relaxation time exceeded 11.6 hours did not fully reorganize into oval shapes within 1000 hours or did not visibly reorganize at all, and simulations with relaxation time below 3.5 hours were unstable with time increments below 15 minutes. In general, offset grafts with high offset distance were more likely to display instability. Relaxation time is the threshold at which viscoelastic materials switch from being dominated more by solid, elastic properties to being dominated by more fluid, viscous properties. It is not surprising, therefore, that as relaxation time increases, the time to reorganize also increases.

A second parameter that affected the model's ability to reorganize to a stable oval shape was muscle force, defined in the model as

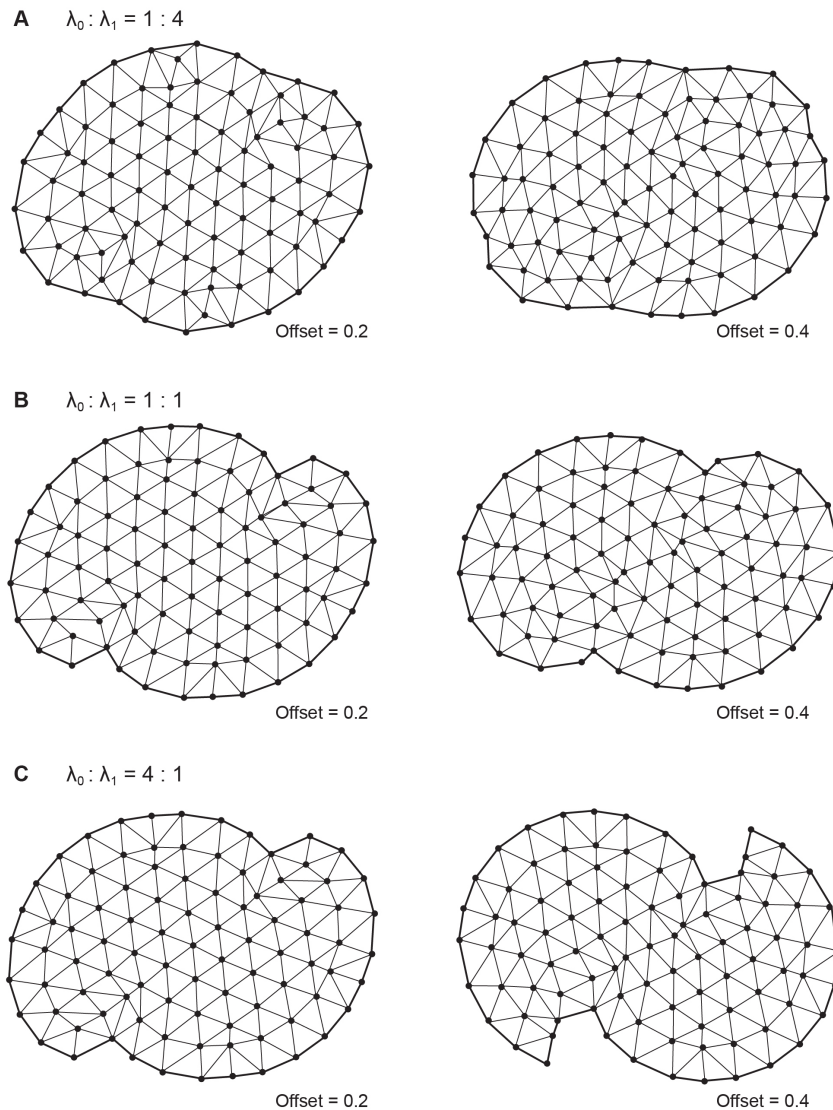$$F_m = \varepsilon_m(\lambda_0 + \lambda_1).$$

Figure 4.1: Reorganization into oval shapes depends on viscoelastic properties. A. Offset grafts after 1000 simulated hours of reorganization when the ratio of λ_0 to λ_1 is 1:4, B. when the ratio of λ_0 to λ_1 is 1:1, and C. when the ratio of λ_0 to λ_1 is 4:1.

Specifically, the ratio between the force produced by the muscle and the viscosity of the material,

$$\frac{\varepsilon_m(\lambda_0 + \lambda_1)}{\eta}$$

was between $0.4 * 10^{-6} 1/s$ and $0.3 * 10^{-5} 1/s$ in all parameter sets that reorganized. When this ratio was too low, reorganization in simulated offsets was often incomplete, and when the ratio was too high, we observed model instability at time increments of 15 minutes, especially at higher offset distances. This supports our hypothesis that force from muscle contraction is the primary driver of reorganiza-

tion. While we are unable to directly measure the magnitude of muscle force in our grafted animals, this result is in line with our experimental observations that animals with higher contraction rates reorganize more quickly.
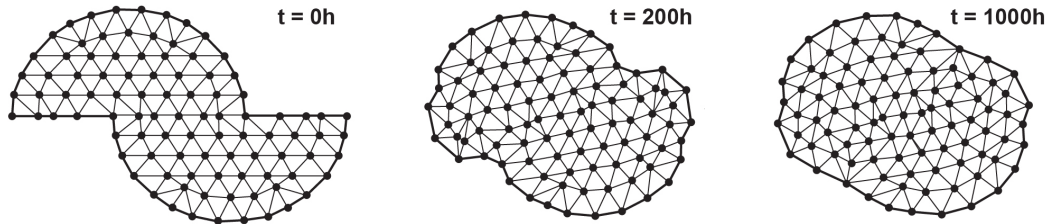

Figure 4.2: Simulation of an offset graft at different time points showing dramatic shape reorganization occurring between 0-200 hours, and gradual boundary smoothing while global shape is stable between 200-1000 hours.

That our simulations were able to recapitulate reorganization to stable oval shape with just local mechanical interactions between muscle contraction and viscoelastic response further supports the model of jellyfish shape as a dynamic equilibrium, as the way muscle and elastic forces are calculated and applied does not change after a stable shape is reached. While we did not explicitly measure through experiments whether muscle force and viscoelastic properties in our offset grafts change to stop reorganization and generate stable shapes, our simulations show that such changes are not necessary to stabilize non-circular animal shapes.

4.2 A single parameter paradigm can produce multiple stable jellyfish shapes given multiple initial geometries

Our grafting experiments showed that Aurelia medusa are able to reorganize into multiple possible stable shapes depending on the initial graft geometry. In the offset grafts, we observed no distinct threshold offset distance at which animals could no longer recover circular body shape. Instead, as offset distance gradually increased, there was a corresponding increase in aspect ratio of the stable oval solutions. In our simulations, we found that there were indeed certain parameter paradigms that were able to recapitulate a relationship between initial offset ratio and stable oval body shape in which the final aspect ratio increased with offset ratio (Figure 4.3A-B). These simulations reached 80% of their final aspect ratio at between 200-500 hours of simulation time and were fully stable by 700 hours of simulation time, after which we observed minor fluctuations in aspect ratio but no dramatic change over time. That oval shapes could be stable at various aspect ratios indicated that a single parameter set could have multiple stable shape equilibria,

depending on initial geometry (Figure 4.3C). Surprisingly, these parameter sets even recapitulated our experimental observations that chimerae can reorganize into S-shaped and asymmetrical animals at high offset distances, though methodology for calculating muscle force and viscoelastic properties did not change (Figure 4.3D).
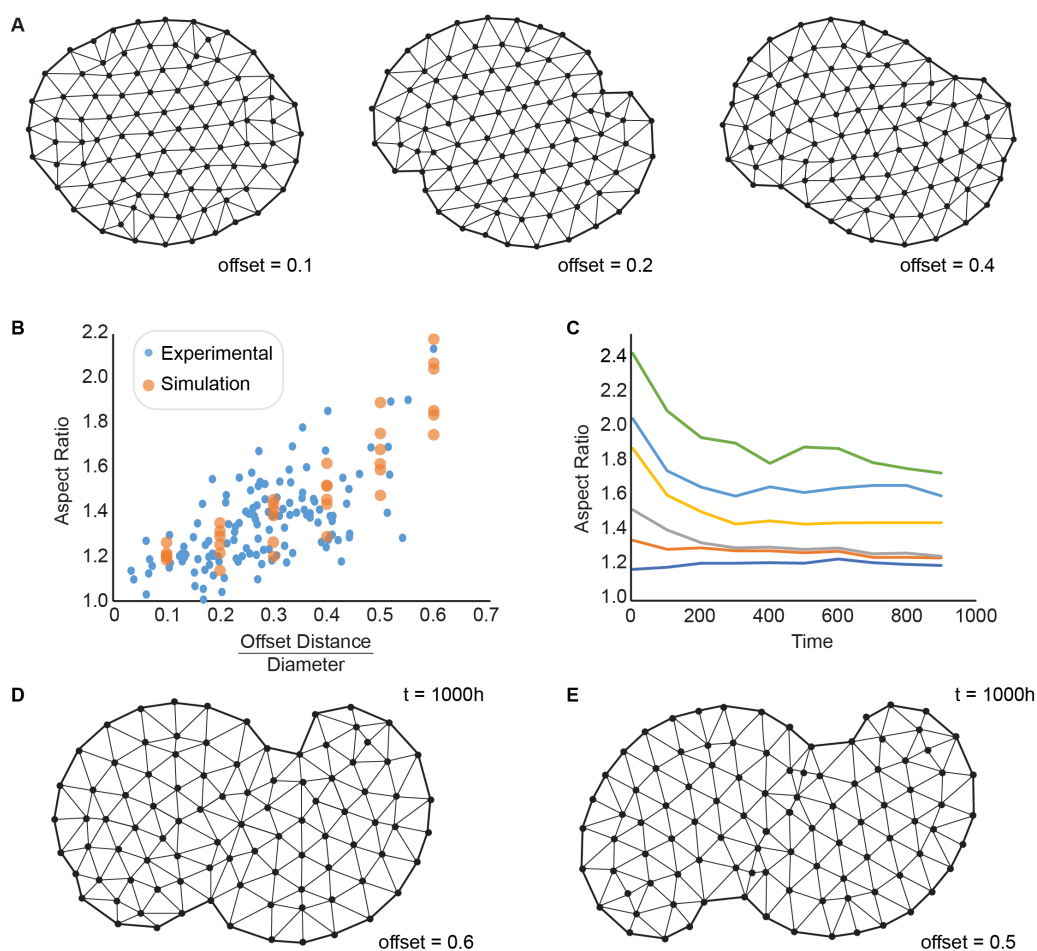

Figure 4.3: Simulation of the offset graft at various offset distances. A. Stable oval solutions of simulated offset grafts at different initial offset distances (t = 1000 hours) B. Relationship between offset distance and final aspect ratio in experimental offset grafts and simulated offset grafts of different offset distances. Experimental data is the same as in Figure 2.4H. C. Evolution of aspect ratio over time in six simulated offset grafts of different offset distances showing that simulated offset grafts eventually reach stable oval shapes. D. A simulated offset graft that reorganized into a stable half oval, half S-shape. E. A simulated offset graft that reorganized into an S-shape.

Thus far we have only simulated reorganization of offset grafts. Can the same parameters also recapitulate reorganization into stable shapes from other graft configurations? We found that when the butterfly graft was set as the initial geometry,
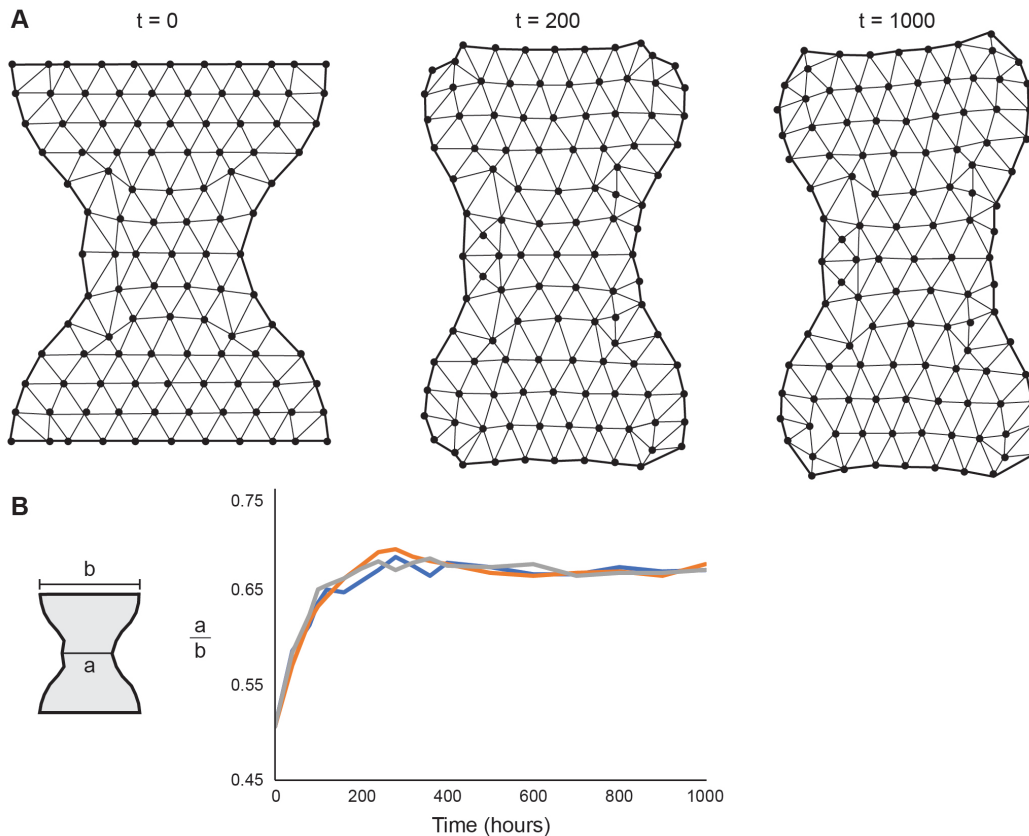
Figure 4.4: Simulation of a butterfly graft. A. Simulation of the reorganization of a butterfly graft into a trapezoidal body shape. The same parameters were used as in Figure 4.3B. B. Reorganization in butterfly grafts was tracked using the ratio of the center width, a, to the wing width, b. Reorganization completed in simulated butterfly grafts between 200-320 hours of simulation time.

simulated grafts in the same parameter paradigms that recapitulated reorganization of offset grafts were also able to reorganize into stable rectangular shapes (Figure 4.4). Reorganization in the butterfly graft was measured by the change in the ratio of the width in the middle of the graft to the width at the widest part of the graft. The timescale of reorganization was 200-320 hours of simulation time with 80% of reorganization completed between 100-120 hours. Even though the muscle configuration in the butterfly graft is very different from the offset graft, a single algorithm for calculating muscle contraction force and viscoelastic response was sufficient to reproduce shape reorganization from both initial geometries into different stable shapes.

4.3 Final stable shape depends on muscle force parameters

Our experimental results indicated that increased contraction rate increased the rate of reorganization. We wondered whether increasing the contraction rate would have a similar effect in our simulated offset grafts. Muscle contraction rate is incorporated into the simulation by increasing the fraction of time muscle force is applied in each time increment. In the simulation results described thus far, the muscle contraction rate was set at 20 contractions per minute, which we had found to be the average contraction rate of our offset grafts. In these simulations, we tested a range of contraction rates between 5 and 55 contractions per minute, equivalent to animals spending 7-73% of the time in a contracted state. 91% of the animals in our graft experiments had contraction rates within this range.

In these simulations of the offset grafts, we found that contraction rate affected the final aspect ratio of the stable oval shapes. Offset grafts with the same initial offset distance reorganized into more elongated oval shapes at low contraction rates and more circular shapes at high contraction rates (Figure 4.5A). We tested this experimentally by creating offset grafts in animals across the range of naturally-occurring contraction rates as well as in animals kept in reduced magnesium seawater, which further widened the range of observed contraction rates. The contraction rate of offset grafts measured at day 1 and day 4 post-surgery was used to calculate the average contraction rate during the reorganization period. Offset grafts were classified by contraction rate into low (<20 contractions per minute) and high contraction rate (>20 contractions per minute) groups. The initial offset ratio and final aspect ratio of these grafts were tracked. We found that while increased offset ratio resulted in more elongated oval animals in both groups, the slope of the offset ratio-aspect ratio relationship was much higher in low contraction rate animals, suggesting that an increase in muscle contraction drives reorganization into more circular animals (Figure 4.5B-C). Indeed, at contraction rates above 35 contractions per minute, we observed very few oval animals with aspect ratio above 1.5 regardless of initial offset (Figure 4.5E). Simulated offset grafts also displayed this phenomenon when contraction rate was varied and all other parameters were held constant, with only oval shapes with low aspect ratios appearing in simulations at high contraction rates (Figure 4.5D).

These simulation and experimental results suggest that not only do changes in parameters such as mechanical stress and viscoelastic properties influence the ability of an *Aurelia*-like system to reorganize and to find stable shapes, but that they can also

influence the speed of reorganization and available shape solutions of the dynamical system.

However, while contraction rate is the only muscle-related parameter that we can vary experimentally, it is not the only parameter needed to characterize muscle contraction force. We are not able to experimentally modulate parameters such as contraction strain, but these are parameter spaces we can explore through our simulations. In our model, contraction strain is not only integrated into calculations of the magnitude of muscle force, but also into the direction of muscle force. Increased contraction strain represents more extreme shortening of the muscle band in the circumferential direction during contractions as well as an increased magnitude of muscle force relative to elastic and pressure forces. When all other parameters are maintained, we found that offset simulations did not fully reorganize at low muscle strains. At higher muscle strains, offset grafts fully reorganized into stable ovals with high aspect ratio (Figure 4.6A). Further increasing muscle strain from this point caused offset simulations to reorganize into ovals with decreased aspect ratio (Figure 4.6B). While this increased circularity in the final stable shape might be the result of an increase in the magnitude of the muscle force, increasing the circumferential muscle strain also changes the geometry of the contracted muscle and direction of muscle force, decreasing the $d\theta$ of muscle contraction (Figure 3.5B). With our current implementation of how muscle force is calculated, we are unable to determine which of these effects on muscle contraction causes the observed change to final stable shape.

4.4   Conclusion

Our simulation results indicate that local mechanical interactions are indeed sufficient to explain jellyfish shape reorganization, as simulated offset and butterfly grafts do display shape change in the absence of cellular processes and global feedback. However, reorganizational ability seems to require a specific range of muscle contraction force and viscoelastic properties. Muscle contraction force above a certain threshold was required for full reorganization, and muscle forces below that threshold resulted in incomplete or no reorganization whatsoever. The viscoelastic properties required for shape change were of particular interest. First, perhaps unsurprisingly, we only observed full reorganization by 1000 hours of simulation time when relaxation time was below a certain threshold. More interestingly, the fluidity of the material was crucial for shape change. When we modeled the viscoelastic behavior as being closer to a Kelvin-Voigt material, the ability of the simulation to
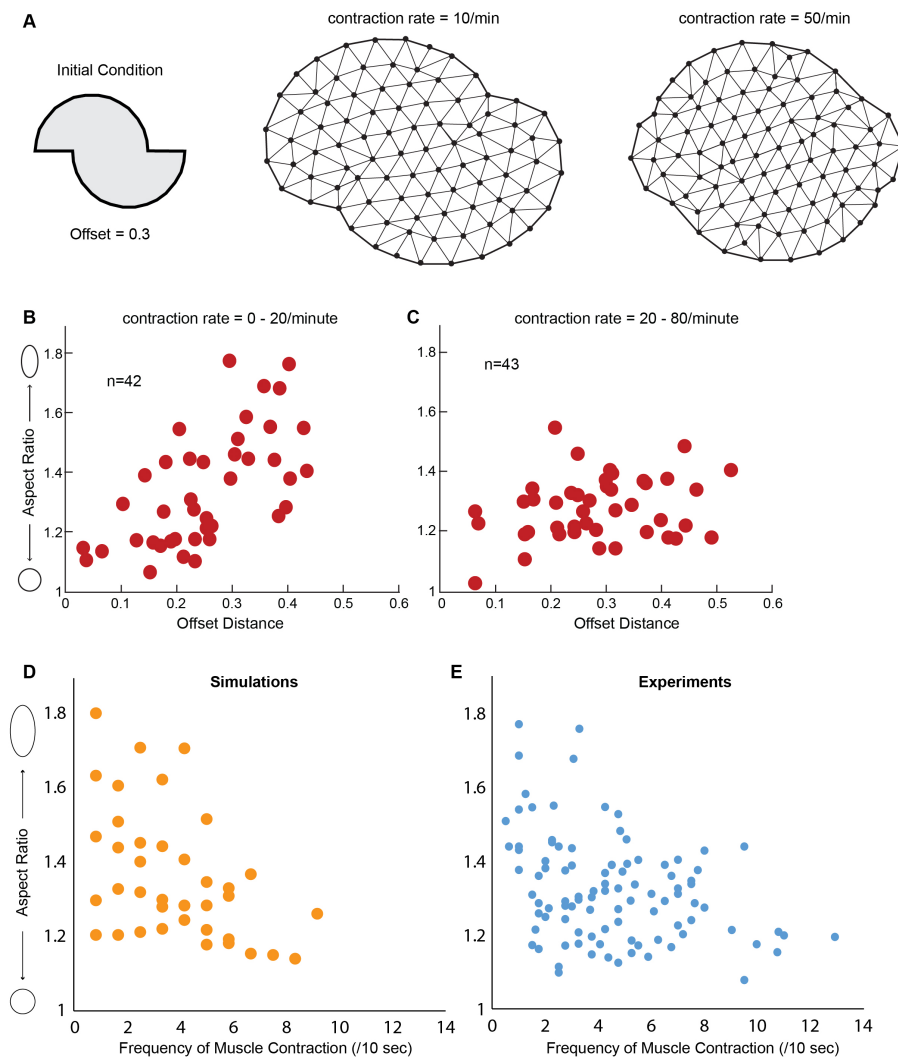
Figure 4.5: Final aspect ratio of real and simulated offset grafts depends on contraction rate. A. Increasing the contraction rate of offset grafts with the same initial offset distance results in more rounded oval solutions. B. Offset ratio vs. final aspect ratio in offset grafts with contraction rate between 0-20 contractions per minute. C. Offset ratio vs. final aspect ratio in offset grafts with contraction rate between 20-80 contractions per minute. D. Contraction rate vs. final aspect ratio in simulated offset grafts. E. Average contraction rate vs. final aspect ratio in offset graft experiments.

reorganize shape was severely limited. A more Maxwell-like model was required to recapitulate shape change to the degree we observed experimentally.

In general, the parameter sets that produced stable oval shapes all displayed a direct relationship between initial offset ratio and final aspect ratio. We found that there existed parameters that could reproduce the specific relationship between offset
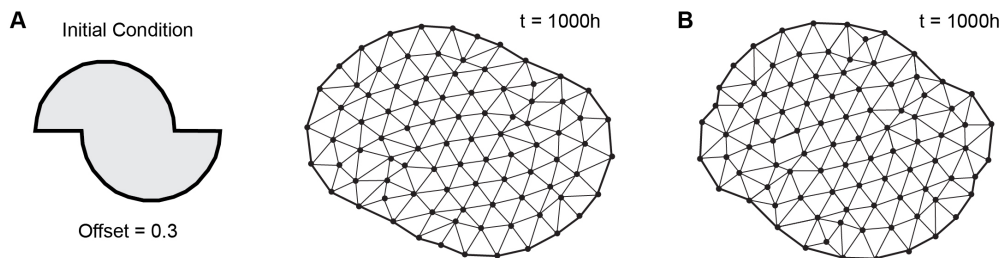
Figure 4.6: Increased muscle force results in rounder solutions from offset grafts. A. A simulated offset graft with offset ratio 0.3 reorganizes to an oval shape at ε_m=0.2. B. A simulated offset graft with the same initial condition reorganizes to a more rounded oval shape at ε_m=0.25.

ratio and aspect ratio that we observed in the offset graft experiments. Some of these parameter sets also produced stable asymmetrical and S-like shapes from high offset initial geometries similar to what we observed at high offset ratio in our offset experiments. The parameter sets that capture this relationship could generally also produce stable rectangular shapes from butterfly geometries. This suggested that rulesets describing the local mechanical interactions are not specific to producing any one stable shape, but rather that a single set of mechanical interactions is able to produce a range of stable jellyfish shapes. Lastly, we found that mechanical parameters like muscle force and contraction rate can also change or limit the possible stable solutions available to the system. Increases to muscle strain and contraction strain resulted in more circular solutions from the same initial geometries. This raises the possibility that a synthetic material could be designed with the right material properties to also change shape flexibly based on the configuration of mechanical forces.

References

Brodland, G. Wayne (2015). "How computational models can help unlock biological systems." In: *Seminars in Cell Developmental Biology* 47, pp. 62–73.

Sugimura, Kaoru, Pierre–François Lenne, and François Graner (2016). "Measuring forces and stresses *in situ* in living tissues." In: *Development* 143, pp. 186–196.

Chapter 5

CONCLUSIONS

In this thesis, I explored a mechanism for shape regulation in the moon jellyfish, *Aurelia aurita*, first experimentally in Chapter 2 and through simulations in Chapters 3 and 4. Through these dual avenues, we found evidence that body shape in *Aurelia* is continuously reinforced through the local mechanical interactions in its body tissues that are created as it propels itself through the water, thus finally answering the question of why jellyfish are round.

That we eventually came up with any kind of answer to this question at all is, frankly, an astonishment. "Why are jellyfish round?" is the kind of question a 5 year-old might come up with, and not a question a "serious scientist" might ask. To understand just *why* it has not been a question for scientific study required some extensive soul-searching. Perhaps the concept of animal shape was just too vague and too simple to warrant investigation, and yet here was an animal for which body shape was functional, that had a mechanism in place to robustly and efficiently repair its shape, and in which body shape could not be taken for granted. Perhaps there are other systems in which shape should not be taken for granted.

In the original study of symmetrization, Abrams et al. found that other species of Scyphozoans, the class of Cnidarians to which *Aurelia* belongs, also recover radial symmetry in the same way, suggesting that the ability to reorganize into novel body shapes might not be unique to *Aurelia*. Homologous mechanisms for shape regulation might also be found outside of soft-bodied animals, since the two main components that drive reorganization in *Aurelia* are ubiquitous in biological systems. All biological materials, even bones, are viscoelastic to some extent (Fung, 1993; Currey, 2002), and these materials are all regularly subject to mechanical forces. Recent research has shown that mechanical forces and material properties play an important role during morphogenesis (Savin et al., 2011; Grosberg et al., 2011; Carter et al., 2004), and the results presented in this thesis suggest that this role does not stop post-development. We have, in fact, examples of this. Gravity compresses our intervertebral disks throughout the course of the day, resulting in the loss of around 2 cm of height, which is then restored at night. Periodic contractions reorganize the local collagen network and dilate the cervix during labor (Ludmir

and Sehdev, 2000). The mechanism for shape regulation in *Aurelia* could give us a framework for understanding what role mechanical forces play in shape regulation, especially of load-bearing and contractile tissues and organs.

In *Aurelia*, too, there are lingering questions about the effects of this mechanism. In this work, we focused on how the mechanical interactions change the shape of the animal when that shape is perturbed by grafting. Furthermore, we focused here on shape changes within the plane of the bell, as these were most dramatic and easy to measure in the short term. However, both our experimental and simulation results indicate that shape regulation is active even during normal physiological function, and we have observed in our animals that bell curvature increases with age. The muscle band, too, widens with age until in some cases it lines the entire subumbrellar surface of the bell. Might repeated mechanical stress from swimming also facilitate shape change and muscle reorganization in this normal physiological context as well?

Lastly, the mechanism described in this study could spark innovation in the field of bio-inspired design, where biological materials have been imitated for their tendency to be softer, stronger, more extensible, and more biocompatible than their engineered counterparts (Joshi et al., 2013; Cheng et al., 2015; Rus and Tolley, 2015; Capadona et al., 2008). Recent advances in materials science has led to the development of materials with self-healing, shape memory, and shape changing properties, but thus far these materials lack the flexibility, autonomy, and dynamism displayed by shape reorganization in Aurelia (Cangialosi et al., 2017; South and Lyon, 2010; Chen et al., 2012; Mynar and Aida, 2008; Phadke et al., 2011; Zhao et al., 2016; Li and Shojaei, 2012). Our modeling results indicate that Aurelia tissue might be an example of a material capable of changing shape on a purely mechanical basis. Further characterization of this material and mechanism could pave the way toward dynamically shape-changing synthetic materials.

BIBLIOGRAPHY

Cangialosi, Angelo et al. (2017). "DNA sequence-directed shape change of pho-topatterened hydrogels via high degree swelling." In: *Science* 357, p. 1126.

Capadona, Jeffrey R. et al. (2008). "Stimuli-reponsive polymer nanocomposites inspired by the sea cucumber dermis." In: *Science* 319, pp. 1370–1374.

Carter, Dennis R. et al. (2004). "The mechanobiology of articular cartilage development and degeneration." In: *Clinical Orthopaedics and Related Research* 427, S69–S77.

Chen, Yulin et al. (2012). "Multiphase design of autonomic self-healing thermoplastic elastomers." In: *Nature Chemistry* 4, pp. 467–472.

Cheng, Qunfeng et al. (2015). "Learning from nature: construction integrated graphene-based artificial nacre." In: *ACS Nano* 9, pp. 2231–2234.

Currey, John (2002). *Bones: Structure and mechanics.* Princeton University Press.

Fung, Yuan–Cheng (1993). *Biomechanics: Mechanical properties of living tissues*. Springer, New York.

Grosberg, Anna et al. (2011). "Self–organization of muscle cell structure and function." In: *PLOS Computational Biology* 7, e1001088.

Joshi, Keyur et al. (2013). "*Aurelia aurita* inspired artificial mesoglea." In: *Integrated Ferroelectrics* 148, pp. 53–66.

Li, Guoquiang and Amir Shojaei (2012). "A viscoplastic theory of shape memory polymer fibres with application to self-healing materials." In: *Proceedings of the Royal Society A* 468, pp. 2319–2346.

Ludmir, Jack and Harish M. Sehdev (2000). "Anatomy and physiology of the uterine cervix." In: *Clinical Obstetrics and Gynecology* 43, pp. 433–439.

Mynar, Justin L. and Takuzo Aida (2008). "The gift of healing." In: *Nature* 451, pp. 895–896.

Phadke, Ameya et al. (2011). "Rapid self-healing hydrogels." In: *PNAS* 109, pp. 4383–4388.

Rus, Daniela and Michael T. Tolley (2015). "Design, fabrication and control of soft robots." In: *Nature* 521, pp. 467–475.

Savin, Thierry et al. (2011). "On the growth and form of the gut." In: *Nature* 476, pp. 57–62.

South, Antoinette B. and L. Andrew Lyon (2010). "Autonomic self-healing of hydrogel thin films." In: *Angewandte Chemie International Edition* 49, pp. 767–771.

Zhao, Qian et al. (2016). "Shape memory polymer network with thermally distinct elasticity and plasticity." In: *Science Advances* 2, e1501297.